Spaceborne Differential GPS Applications

Final Technical Report

NRL Scientific Officer :   Robert Dasenbrock

Principal Investigator: Penina Axelrad
Graduate Students: Dolan Highsmith, Angela Reichert

Colorado Center for Astrodynamics Research
University of Colorado, CB 431
Boulder, CO 80309-0431

February 17, 2000

20000224 165

Abstract

This final technical report summarizes the research performed by the Colorado Center for Astrodynamics Research (CCAR) for the Naval Research Laboratory (NRL) on Spaceborne Differential GPS Applications over the period 01 September 1997 through 31 August 1999. The primary focus of our work was on relative state estimation using GPS data from two vehicles. Data from a spaceborne experiment conducted by NASA was used for algorithm development and performance analysis. An auxiliary area of research was the identification and reduction of multipath errors in GPS observations. This effort is key to full utilization of GPS for high precision applications such as attitude determination, differential GPS, and relative navigation. The report comprises three documents describing the research. The first two are conference papers presented at ION GPS 99 describing the relative navigation and multipath research. The third is a doctoral dissertation research proposal written by Dolan Highsmith, summarizing his research on this project and plans for future work.

Relative State Estimation Using GPS Flight Data from Co-Orbiting Spacecraft

Dolan Highsmith *Naval Research Laboratory*
Penina Axelrad *University of Colorado, Boulder*

BIOGRAPHY

Dolan Highsmith received a B.S. in Aerospace Engineering from the University of Virginia in 1993, and an M.S. in the same field from the University of Colorado at Boulder in 1997. He is currently pursuing a Ph.D. in Aerospace Engineering from CU Boulder as a co-op at the Naval Research Laboratory in Washington, D.C.

Penina Axelrad is an Associate Professor. Her research is focused on GPS technology and applications. Dr. Axelrad received her Ph.D. in Aeronautics and Astronautics from Stanford University and her S.M. and S.B. from M.I.T.

ABSTRACT

The objective of this research is to use flight data to develop and demonstrate the most accurate and robust GPS-based methods for relative navigation for two co-operative, co-orbiting vehicles in LEO. A Kalman filter that directly estimates the relative state between two co-orbiting vehicles using single difference pseudo-range observations has been developed. This filter is used in conjunction with an existing GPS absolute orbit determination utility, which provides an estimate of the absolute orbit of the passive vehicle to the relative filter. The Clohessy-Wiltshire equations are used for state and error propagation. This filter has been designed using flight data from the STS-80/ORFEUS-SPAS flight experiment performed in December 1996. The root-mean-square (RMS) relative position errors are 6.4 m radial, 5.3 m in-track, and 1.3 m cross-track. The RMS velocity errors are 0.022 m/s radial, 0.018 m/s in-track, and 0.013 m/s cross-track. Though the relative positions are no better than NASA/JSC results, this fairly simple filter achieved an overall improvement of more than 70% in relative velocity. This is an excellent beginning upon which to build future

adaptations, which may include relative J2, relative drag, and carrier phase processing.

INTRODUCTION

Accurate relative navigation of spacecraft permits capabilities such as rendezvous and formation flying—key aspects of many current and future space missions. In low earth orbit (LEO), such missions can use the Global Positioning System (GPS) signal as the primary navigational aid for relative positioning. For example, GPS relative navigation can be used for rendezvous operations at the International Space Station and for precise positioning of distributed, coordinated remote sensing satellites. Such applications require highly accurate knowledge of the relative orbits. However, previous work in the application of GPS to relative navigation in space has not demonstrated on actual flight data the performance required for precise applications. Therefore, the objective of this research is to use flight data to develop and demonstrate the most accurate and robust GPS-based methods for relative navigation for two cooperative, co-orbiting vehicles in LEO.

A Kalman filter that directly estimates the relative state between two co-orbiting vehicles using single difference pseudorange observations has been developed. This filter is used in conjunction with an existing GPS absolute orbit determination utility, which provides an estimate of the absolute orbit of the passive vehicle to the relative filter. Use of single difference pseudoranges reduces errors inherent in using GPS by removing common mode errors, such as the satellite clock error. Furthermore, directly estimating a relative state allows the use of the Clohessy-Wiltshire (CW) equations for state and error propagation. In fact, in its current form the relative filter requires no integration.

Specifically, this filter estimates a relative position and velocity and relative receiver clock bias and drift.

It uses the CW equations with velocity aiding to propagate the position and velocity, incorporating the absolute orbit estimate of the passive vehicle to compute the mean motion. The CW equations are also used to propagate the covariance. The measurement update computes the observed and predicted single difference pseudoranges, where the predicted quantity accounts for the body-fixed GPS antenna offset from the center of gravity by using a reported attitude estimate.

Previous GPS relative navigation research using flight data has concentrated on determining the relative orbit by differencing two absolute orbits. Schiesser et al. implemented such a filter for the Shuttle/ORFEUS-SPAS relative navigation experiment during the STS-80 mission in December 1996 [1]. Their filter uses GPS coarse/acquisition (C/A) code pseudoranges to solve for the absolute orbits of the two vehicles, then differences them to form the relative orbit. Unlike a relative state filter which must interpolate asynchronous observations taken from the different receivers, the absolute orbit differencing method does not require interpolation, nor does it necessarily require observations from common GPS satellites.

More recently, D'Souza et al. from Draper Lab developed a filter very similar to the one presented here for use with two NASDA projects, Engineering Test Satellite 7 (ETS-VII) and the H-II Transfer Vehicle (HTV) [2]. Excellent simulation results were obtained. Presuming NASDA implemented this filter for ETS-VII, Mokuno et al. indicate that on-orbit results were also good, obtaining a GPS-derived relative range within 1 m of the rendezvous radar measurement and an in-plane velocity error within 2 cm/s [3]. The major difference between the Draper filter and the one developed in this paper is the dynamic model used for state propagation. The Draper filter uses a fourth-order Runga-Kutta integrator with J2, J3, J4, and drag to integrate the absolute states for both vehicles, then creates the relative state from their difference. Though undoubtedly more accurate than the linear, unperturbed CW propagation used here, the CW propagation was found to be sufficient for measurement intervals of ten seconds or less, with fast recoveries after large data outages.

The following sections describe the development of the relative state filter using the flight data from the STS-80 rendezvous experiment.

FLIGHT EXPERIMENT

The STS-80 mission launched November 19, 1996, and returned to Earth December 7, 1996. During the mission, the Space Shuttle Columbia released the free-flying Orbiting and Retrievable Far and Extreme Ultraviolet Spectrograph Shuttle Pallet Satellite (ORFEUS SPAS). Both the SPAS and the Shuttle had GPS receivers on board, which were used to record concurrent observations for demonstration of relative navigation using GPS. The SPAS had a nine-channel Laben Tensor GPS receiver with four antennas, while the Shuttle used a six-channel Trimble Advanced Navigation System Quadrex GPS receiver with two antennas mounted across the payload bay [1].

The data set used in this work comprises the final 73 minutes of rendezvous, up to the capture (grapple) of the SPAS with the Shuttle robotic arm. Several data sets were taken throughout the mission, but only the rendezvous portion had a valid relative orbit truth reference. This segment of the experiment employed a laser on the Shuttle for determining range and range-rate to the SPAS. These data were converted into a best estimated relative trajectory (BERT) in radial, in-track, and cross-track (RIC) coordinates.

Because of the frequent thrusting of the Shuttle during rendezvous, the filter includes compensation for the delta-V maneuvers. Given Shuttle delta-V vectors expressed in RIC coordinates, implementation of velocity aiding in the filter is straightforward. The delta-V measurements were produced by the Shuttle IMU accelerometer, which reported accumulated sensed velocity [1].

Since the relative navigation filter relies on single difference pseudoranges, only common-view GPS satellite observations may be used. Fortunately, the rendezvous phase of the flight was performed in such as way as to maximize the potential for common view satellites. The Shuttle payload bay remained pointed at the SPAS so the crew could maintain visual contact; consequently, the SPAS was commanded to pitch at a constant rate so that its GPS antennas pointed in approximately the same direction as those on the Shuttle throughout the rendezvous [1].

OBSERVATIONS

Both GPS receivers reported C/A code phase, L1 carrier phase, and L1 Doppler. The filter described in this paper uses the C/A code pseudoranges from each common-view GPS satellite to create the single differ-

ence observation. The receivers were not synchronized, so the measurement time tags are different. Therefore, the pseudoranges from the active vehicle (Shuttle) receiver are interpolated to the times of the passive vehicle (SPAS) pseudoranges using polint.c, a polynomial interpolation routine from *Numerical Recipes* [4]. Polint.c uses Neville's algorithm to construct the interpolating polynomial. As implemented in the filter, the desired point is computed between the second and third values of a four-point interpolation.

Given a noise level on each C/A code pseudorange of approximately 3 meters, interpolated points between four closely-timed observations will also be noisy. This effect contributes to large measurement residuals obtained using these data. A potential remedy for the large noise, short of using carrier phase pseudoranges, is carrier interpolation or carrier smoothing of the C/A code pseudoranges. Preliminary results using these methods, however, do not show sufficient improvement to warrant inclusion in this paper.

RELATIVE STATE KALMAN FILTER

Overview

The relative state s_r consists of a relative position r_r and velocity v_r, as well as relative receiver clock bias b_r and frequency f_r, such that

$$s_r = \begin{bmatrix} r_r^T & v_r^T & b_r & f_r \end{bmatrix}^T. \tag{1}$$

The relative state is referenced to the passive vehicle (SPAS). The filter position and velocity coordinate frame is centered on the passive vehicle and expressed in radial, in-track, and cross-track directions. Likewise, the covariance and process noise values are specified for the RIC directions. This formulation permits more direct use of the CW equations for state and covariance propagation.

Input data to the Relative State Kalman Filter (RSKF) include asynchronous GPS code pseudoranges for both vehicles, absolute orbit estimates for the passive vehicle, and GPS satellite position vectors. Since the RSKF is designed to work in tandem with an external GPS absolute orbit determination (AOD) utility, output from it is used as input to the RSKF. The external AOD program generates the absolute orbit estimates of the passive vehicle using GPS code pseudoranges and broadcast GPS satellite orbits. The orbit estimates, along with the GPS observations and satellite positions used to compute them, are output from the AOD program for use as input to the RSKF. As mentioned previously, within the RSKF the active vehicle pseudoranges are interpolated to the times of the passive vehicle pseudoranges and positions.

Inertial-to-body attitude quaternions and delta-V vectors are also input to the RSKF. The attitude quaternions of the Shuttle are needed to account for the GPS antenna CG offsets, which are specified in a body-fixed frame. Since the SPAS attitude mimicked that of the Shuttle, a total relative offset is computed in the Shuttle body frame, which is then rotated to RIC using the Shuttle attitude. The delta-V vectors are used in the time update propagation to account for the thrusting of the Shuttle during rendezvous.

Time Update

As stated previously, the CW equations are used in this filter for relative state and covariance propagation. From Prussing and Conway [5], the CW equations in state transition matrix form are

$$\Phi_{r,v}(\Delta t) =$$
$$\begin{bmatrix} 4-3c & 0 & 0 & \frac{s}{n} & \frac{2(1-c)}{n} & 0 \\ 6(s-n\Delta t) & 1 & 0 & -\frac{2(1-c)}{n} & \frac{4s-3n\Delta t}{n} & 0 \\ 0 & 0 & c & 0 & 0 & \frac{s}{n} \\ 3ns & 0 & 0 & c & 2s & 0 \\ -6n(1-c) & 0 & 0 & -2s & 4c-3 & 0 \\ 0 & 0 & -ns & 0 & 0 & c \end{bmatrix} \tag{2}$$

where n signifies the mean motion of the passive vehicle, Δt is the time interval for propagation, and $s = \sin(n\Delta t)$ and $c = \cos(n\Delta t)$. In the filter, the mean motion in the equation above is actually computed as the angular rotation rate $(\dot{\theta})$ at the current time. In other words, the mean motion is chosen at each epoch to be the current along-track velocity of the passive vehicle divided by its radius. This provides a more accurate propagation for elliptical orbits as long as the measurement interval is not large.

The relative clock frequency is assumed constant over the time interval, so the clock terms are propagated with [6]

$$\Phi_{b,f}(\Delta t) = \begin{bmatrix} 1 & \Delta t \\ 0 & 1 \end{bmatrix}. \tag{3}$$

Thus, the full relative state transition matrix has the form

$$\Phi(\Delta t) = \begin{bmatrix} \Phi_{r,v}(\Delta t) & 0_{6\times2} \\ 0_{2\times6} & \Phi_{b,f}(\Delta t) \end{bmatrix}. \tag{4}$$

Incorporated into the state propagation is velocity aiding, accomplished by using the Δv vectors of the

active vehicle. The velocity vectors are added directly into the linear state propagation at the given time as impulsive maneuvers, with potentially more than one maneuver between measurement epochs. The following example illustrates the equations for the occurrence of one $\Delta \mathbf{v}$ during the interval. As such, the state must be propagated from t_k to t_{k+1} with a maneuver at $t_{\Delta v}$ such that $t_k < t_{\Delta v} < t_{k+1}$. In this case, the state vector is propagated as follows:

$$\mathbf{s}_{\Delta v}^- = \mathbf{\Phi}\left(t_{\Delta v}, t_k\right) \mathbf{s}_k^+ \tag{5}$$

$$\mathbf{s}_{\Delta v}^+ = \mathbf{s}_{\Delta v}^- + \left[\mathbf{0}_{3\times1}^T \ \Delta \mathbf{v}^T \ \mathbf{0}_{2\times1}^T\right]^T \tag{6}$$

$$\mathbf{s}_{k+1}^- = \mathbf{\Phi}\left(t_{k+1}, t_{\Delta v}\right) \mathbf{s}_{\Delta v}^+ \tag{7}$$

where the $^-$ and $^+$ indicate state vector values before or after the measurement update or a maneuver. The distinction is clear from the context.

Not portrayed in the above equations is the fact that the CW state propagation is performed in cylindrical coordinates, with the along-track direction being along the arc of the orbit. Since this filter operates in the rectangular RIC coordinates, a rotation is performed to cylindrical RIC coordinates immediately before each state propagation step (e.g., Eq. 5), then back to rectangular immediately after. The equations for such a conversion are given in [8]. However, for this filter, those equations are re-derived for the case that $\dot{r}$ is not zero, providing a slight increase in accuracy.

Ignoring any potential maneuvers, the covariance is propagated over the entire measurement interval using

$$\mathbf{P}_{k+1}^- = \mathbf{\Phi}\left(t_{k+1}, t_k\right) \mathbf{P}_k^+ \mathbf{\Phi}\left(t_{k+1}, t_k\right)^T + \mathbf{Q}_k. \tag{8}$$

The process noise matrix $\mathbf{Q}$ is derived from Gelb, equation 3.6-13 [7], resulting in the equation

$$\mathbf{Q}_k = \int_{t_k}^{t_{k+1}} \mathbf{\Phi}\left(t_{k+1}, \tau\right) \mathbf{Q}\left(\tau\right) \mathbf{\Phi}^T\left(t_{k+1}, \tau\right) d\tau. \tag{9}$$

where $\mathbf{Q}(t)$ is defined to be the spectral density matrix. Eq. 9 is solved symbolically using Eq. 4 and a diagonal representation of the spectral density matrix $\mathbf{Q}(t)$.

Measurement Update

The RSKF performs a measurement update for each GPS observation separately, so the equations in this section refer to quantities for one common view GPS satellite. Given pseudorange observations to the same GPS satellite from the active receiver ρ_A and passive receiver ρ_P, the single difference observation is simply

$$\rho_{SD} = \rho_A - \rho_P. \tag{10}$$

The predicted single difference pseudorange $\tilde{\rho}_{SD}$ is computed from the geometric relative range, relative clock bias estimate, and antenna CG offsets. Because the pseudoranges in the above equation are measured from the GPS antennas, ρ_{SD} is not referenced to the centers of gravity of the two vehicles. Therefore, the prediction of the single difference pseudorange must account for the antenna CG offset vector $\mathbf{r}_{ANT}$. In the equations below, $\mathbf{r}_{ANT}$ can be viewed as the sum of the antenna offset vectors from the two vehicles.

The geometric relative range is found by differencing the ranges to the active and passive vehicles using the GPS satellite position $\mathbf{R}_{GPS}$, passive vehicle absolute position estimate $\mathbf{r}_P$, and predicted relative position estimate $\tilde{\mathbf{r}}_{REL}$ from the time update. The computed ranges to the active and passive vehicle receivers are

$$\tilde{r}_P = |\mathbf{R}_{GPS} - \mathbf{r}_P| \tag{11}$$

$$\tilde{r}_A = |\mathbf{R}_{GPS} - (\mathbf{r}_P + \tilde{\mathbf{r}}_{REL} + \mathbf{r}_{ANT})|. \tag{12}$$

The predicted single difference is then computed from

$$\tilde{\rho}_{SD} = \tilde{r}_A - \tilde{r}_P + b_{REL}. \tag{13}$$

The single difference pseudorange residual is formed using

$$z = \rho_{SD} - \tilde{\rho}_{SD}. \tag{14}$$

The partial differential of Eq. 13 with respect to the relative state (Eq. 1) produces the measurement gradient matrix $\mathbf{H}$ with the first three elements being

$$H_{11} = -\frac{X_{GPS} - (x_P + \tilde{x}_{REL} + x_{ANT})}{\tilde{r}_A} \tag{15}$$

$$H_{12} = -\frac{Y_{GPS} - (y_P + \tilde{y}_{REL} + y_{ANT})}{\tilde{r}_A} \tag{16}$$

$$H_{13} = -\frac{Z_{GPS} - (z_P + \tilde{z}_{REL} + z_{ANT})}{\tilde{r}_A} \tag{17}$$

so that the full matrix is

$$\mathbf{H} = \left[\ H_{11} \quad H_{12} \quad H_{13} \quad 0 \quad 0 \quad 0 \quad 1 \quad 0\ \right]. \tag{18}$$

The Kalman gain is computed from the equation

$$\mathbf{K} = \mathbf{P}_{k+1}^- \mathbf{H}^T \left(\mathbf{H}\mathbf{P}_{k+1}^- \mathbf{H}^T + \mathbf{R}\right)^{-1} \tag{19}$$

and the covariance is updated with

$$\mathbf{P}_{k+1}^+ = (\mathbf{I} - \mathbf{K}\mathbf{H}) \mathbf{P}_{k+1}^- (\mathbf{I} - \mathbf{K}\mathbf{H})^T + \mathbf{K}\mathbf{R}\mathbf{K}^T. \tag{20}$$

Since the measurement update is performed for each GPS satellite separately, the measurement noise matrix $\mathbf{R}$ is 1×1, so the inversion in Eq. 19 is a simple scalar inversion.

Table 1: Relative orbit position error statistics with respect to laser BERT for the Relative State Kalman Filter and the NASA/JSC filter [1].

Source	m	Rad	In	Cross
RSKF	Mean	-2.8	-4.2	0.2
	STD	5.8	3.2	1.3
	RMS	6.4	5.3	1.3
	RSS		8.4	
JSC	Mean	-1.5	-2.6	-0.2
	STD	7.5	2.9	2.9
	RMS	7.6	3.9	2.9
	RSS		9.0	

Table 2: Relative orbit velocity error statistics with respect to laser BERT for the Relative State Kalman Filter and the NASA/JSC filter [1].

Source	cm/s	Rad	In	Cross
RSKF	Mean	-1.0	-0.4	0.1
	STD	2.0	1.8	1.3
	RMS	2.2	1.8	1.3
	RSS		3.1	
JSC	Mean	-2.0	0.0	-1.2
	STD	8.7	6.1	4.0
	RMS	8.9	6.1	4.2
	RSS		11.6	

Figure 1: In-plane trajectories for filter and laser BERT.

Finally, the relative state is updated by

$$s_{k+1}^{+} = s_{k+1}^{-} + Kz. \qquad (21)$$

The measurement update is repeated for each common view GPS satellite. After exhausting all the observations for this epoch, the next measurements are chosen and the entire process is repeated.

RESULTS & DISCUSSION

Given noisy, asynchronous observations from the drag-laden, maneuvering Shuttle and the relatively well-behaved SPAS, the RSKF obtains excellent results considering its simplicity. In fact, the results are comparable or better than results obtained in a NASA/JSC study detailed in [1]. Tables 1 and 2 show the position and velocity error statistics for the same 73 minute period using the same truth reference (the laser BERT) for the RSKF developed in this paper and the filter developed by JSC. These results are obtained with the following initial variances: 4000, 1000,
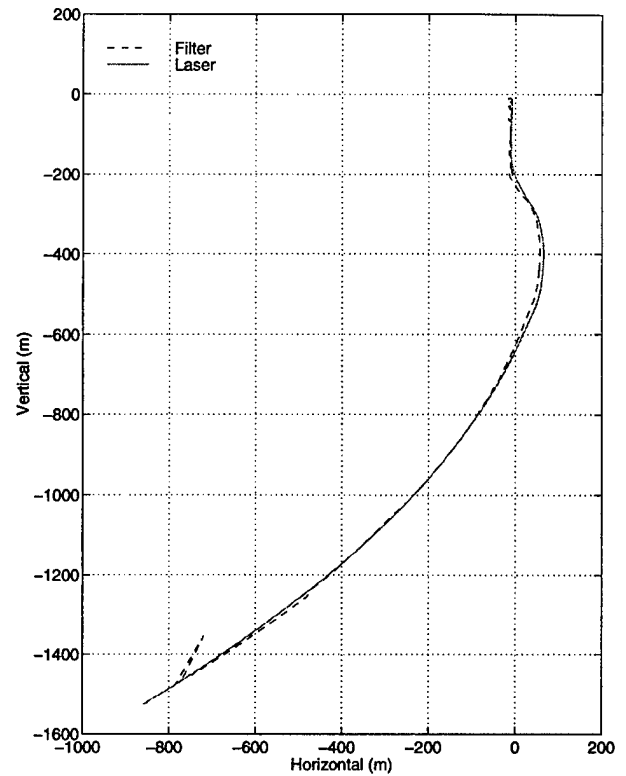
and 100 m^2 for RIC relative position; 0.004, 0.004, and 0.001 m^2/s^2 for RIC relative velocity; 2000 m^2 for relative clock bias; and 25 m^2/s^2 for relative clock frequency. The initial spectral densities are as follows: 1e-5, 4e-6, 8e-6 m^2/s for RIC relative position; 3e-7, 4e-8, 8e-8 m^2/s^3 for RIC relative velocity; 0.01 m^2/s for relative clock bias; and 0.008 m^2/s^3 for relative clock frequency. The noise on the measurement is estimated to be approximately 3 m, so the scalar measurement noise value R is set to 9 m^2. It becomes apparent in subsequent plots that additional tuning must be performed so that the filter 3σ RMS values more accurately reflect the behavior of the system.

To illustrate the nature of the rendezvous, Figs. 1, 2, and 3 show the relative position and velocity states. The in-plane relative trajectories for the filter and laser BERT are shown in Fig. 1. Note that motion is to the right and the Earth is down. It can be seen from this plot that the rendezvous data set begins at a range of approximately 1.8 km and ends at SPAS capture. Figs. 2 and 3 show all the relative position and velocity states as determined by the RSKF and the laser
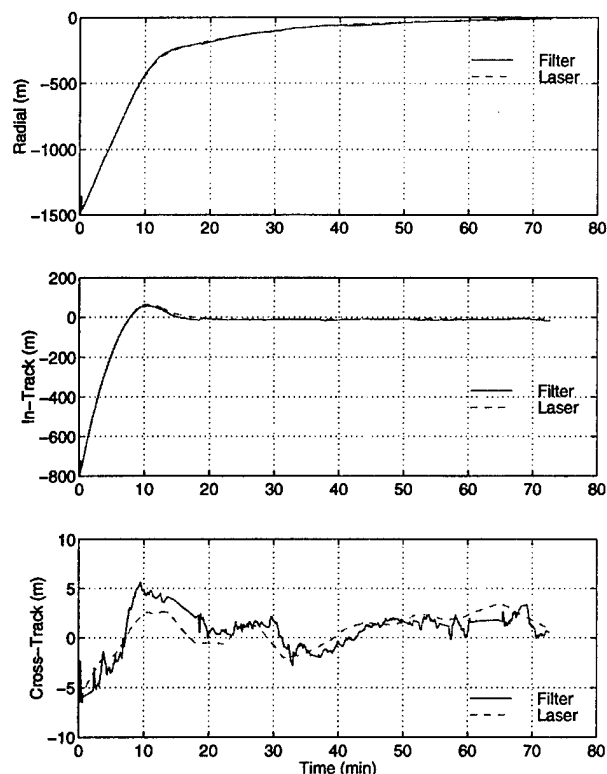
Figure 2: Radial, along-track, and cross-track relative positions for the filter solutions and laser BERT.

Figure 3: Radial, along-track, and cross-track relative velocities for the filter solution and laser BERT.

BERT. These plots reveal the large dynamic motion of the Shuttle during the first fifteen minutes as it narrows the relative range from 1.8 km to 200 m. After the first fifteen minutes, the relative motion becomes fairly benign.

Another indicator of the large motions is the plot of the delta-V magnitudes in Fig. 4. For the purpose of velocity aiding in the RSKF, a range of minimum thresholds was evaluated. A threshold of 1.5 cm/s was determined to provide the best accuracy. The figure shows a line at 1.5 cm/s, with the points above it marked by squares to indicate those used in state propagation.

The relative position errors with respect to the laser BERT in the radial, along-track, and cross-track directions are shown in Fig. 5. The 3σ bounds determined by the RSKF variances are shown as the dashed lines. Fig. 6 shows the relative velocity errors with respect to the laser BERT. Again, the 3σ bounds determined by the filter variances are shown as the dashed lines. Compare the behavior of these error plots with the mo-
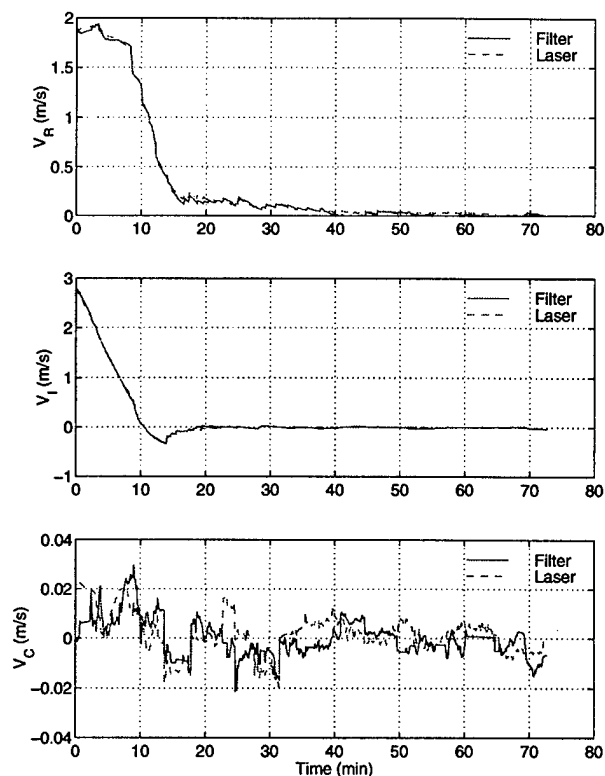
tion shown in Figs. 2 and 3. Clearly, the RSKF has difficulty obtaining accurate results during the highly dynamic motion of the first fifteen minutes, even with velocity aiding. After that period, however, the filter estimates become less erratic.

Notice the biases and systematic variations in the relative position error for the radial and along-track directions. These are reflected in the mean and RMS statistics in Table 1. We are investigating possible sources of error, including inaccurate GPS antenna CG offsets, time tagging errors, or simply unknown/unmodeled biases. The fact remains, however, that these biases can be removed by adjusting the body-fixed antenna CG offsets by the bias amount. Doing so lowers the position RMS errors to the same level as the standard deviations, thereby reducing the total RSS position error from 8.4 m to 6.9 m. There is only a minimal improvement in the velocity statistics.

To ensure that the RSKF CW propagation is not introducing a bias to the results, a hardware-in-the-loop simulation data set used in [9] was used to verify its accuracy. A 5 km along-track separation was simu-
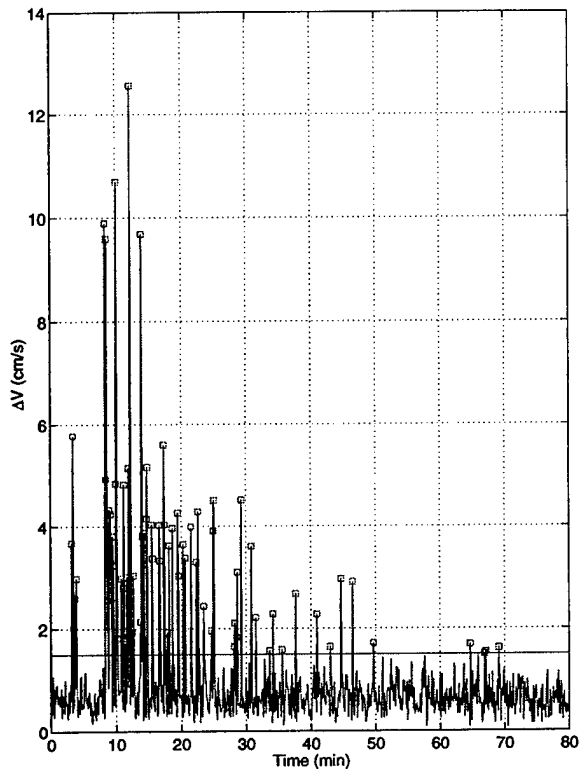
Figure 4: Shuttle IMU-sensed ΔV magnitudes. Threshold of 1.5 cm/s is shown, with squares signifying the points used in state propagation.

Figure 5: Relative position error in radial, along-track, and cross-track directions with respect to laser. Dotted lines show filter 3σ RMS limits

lated, with the receiver reporting P-code pseudoranges without selective availability or multipath. For this low-noise (approximately 3 cm) data set, the RSKF obtained an unbiased relative position RSS of 0.18 m and a relative velocity RSS of 0.5 cm/s. Clearly, the source of the bias in the Shuttle/SPAS data set requires further investigation.

The most dramatic result of this research is the improvement in relative velocity estimates by the RSKF versus the JSC results. The RSKF total RSS velocity error of 3.1 cm/s is a 73% improvement over the 11.6 cm/s value from JSC (see Table 2). Both filters include velocity aiding using the Shuttle IMU accelerometer data. In fact, both filters use virtually the same data, so the improvement in velocity accuracy is most likely an artifact of estimating a relative state as opposed to two absolute states.

The error in relative semimajor axis (SMA) is shown in Fig. 7. This error is computed as the difference between the relative SMA computed with RSKF
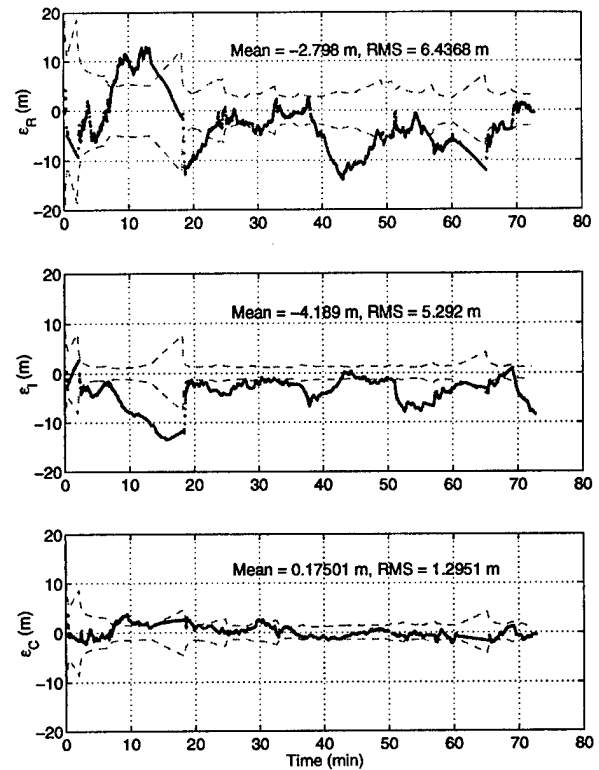
states and the relative SMA computed with the laser BERT. Note that for lack of a valid absolute orbit truth for the passive vehicle, the relative SMA from the BERT is computed using the passive vehicle absolute state from the external AOD filter. Thus, the relative SMA comparison does not include errors due to inaccuracies in the absolute orbit estimate of the SPAS.

CONCLUSIONS

In a relatively simple form, the RSKF has demonstrated on flight data the ability to predict relative position and velocity to accuracy levels comparable to or better than the absolute state filter developed by NASA/JSC. Further improvements in positioning accuracy may be obtained by identifying the source of the relative position estimate biases, which appear in both the RSKF and the JSC filter results to differing degrees. There is also the potential for additional overall improvements in accuracy by implementing a
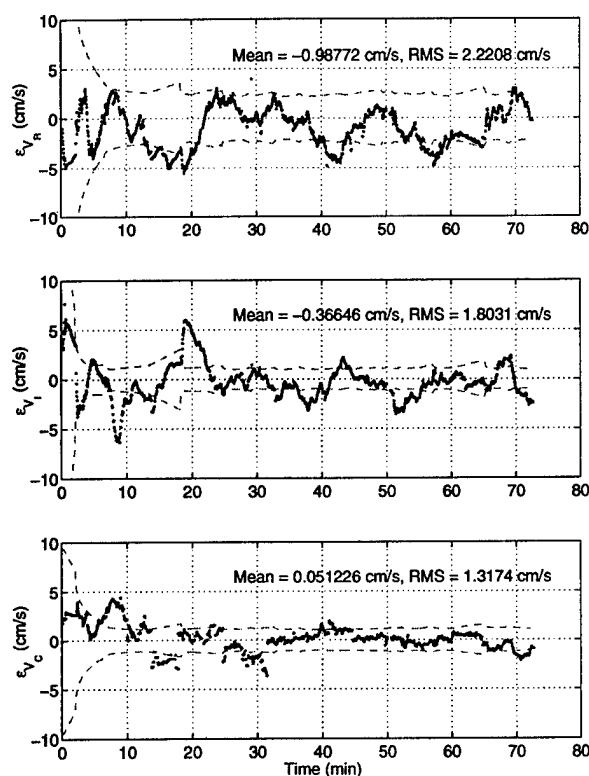
Figure 6: Relative velocity error in radial, along-track, and cross-track directions with respect to laser. Dotted lines show filter 3σ RMS limits
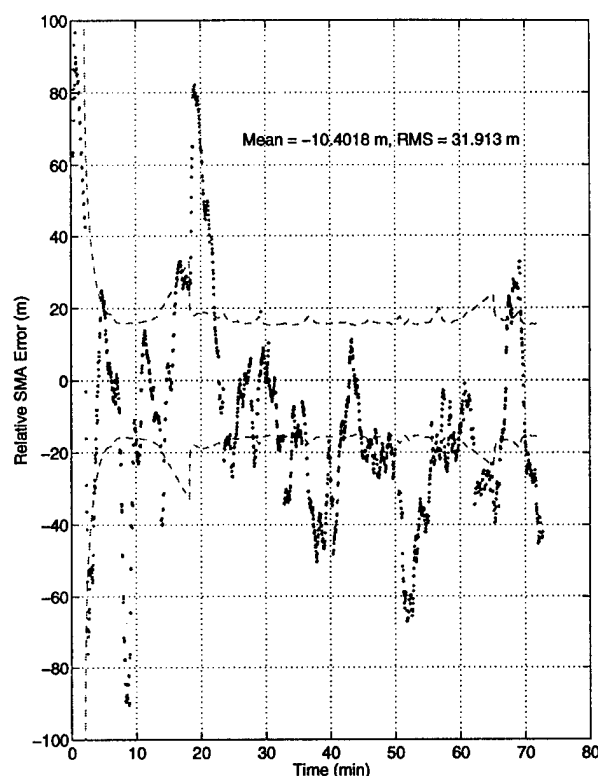

Figure 7: Relative semimajor axis error of RSKF with respect to the laser BERT. Dotted lines show filter 3σ relative SMA RMS limits.

relative state propagator that accounts for the effects of relative gravity and drag perturbations. The most dramatic improvement, however, is gained by using more precise observations and techniques, namely carrier phase processing coupled with synchronization of the vehicle clocks. This is the direction of future research on the RSKF.

ACKNOWLEDGMENTS

REFERENCES

[1] Schiesser, E., Brazzel, J. P., Carpenter, J. R., Hinkel, H. D.,"Results of STS-80 Relative GPS Navigation Flight Experiment," *Proceedings of AAS/AIAA Space Flight Mechanics Meeting*, Paper AAS 98-194, Vol. 99, Part II, 1998.

[2] D'Souza, C., et al., "An Evaluation of the GPS Relative Navigation System for ETS-VII and HTV," 22nd Annual AAS Guidance and Control Conference, February 3-7, 1999.

[3] Mokuno, M., Kawano, I., Kasai, T., "Experimental Results of Autonomous Rendezvous Docking on Japanese ETS-VII Satellite," 22nd Annual AAS Guidance and Control Conference, February 3-7, 1999.

[4] Press, W. H., et al., *Numerical Recipes in C: The Art of Scientific Computing.* Cambridge University Press, Cambridge, 1992.

[5] Prussing, J. E., and Conway, B. A., *Orbital Mechanics*. Oxford University Press, New York, 1993.

[6] Parkinson, B. W., and Spilker, J. J., Jr., eds., *Global Positioning System: Theory and Applications Volume I*. American Institute of Aeronautics and Astronautics, Washington, DC, 1996.

[7] Gelb, A., ed., *Applied Optimal Estimation*. The M.I.T. Press, Cambridge, 1974.

[8] Bond, V. R., "A New Solution for the Rendezvous Problem," Paper AAS-99-178, AAS/AIAA Space Flight Mechanics Meeting, February 7-10, 1999.

[9] Binning, P. W., *Absolute and Relative Satellite to Satellite Navigation Using GPS*. Ph. D. Dissertation, University of Colorado, 1997.

GPS Carrier Phase Multipath Reduction Using SNR Measurements to Characterize an Effective Reflector

Angela Reichert and Penina Axelrad, *University of Colorado*

BIOGRAPHY

Angela Reichert is currently a Ph.D. student at the University of Colorado, Boulder. Her research interests include GPS carrier phase multipath mitigation and orbit and attitude determination using GPS. She received her M.S. in Aerospace Engineering Sciences from the University of Colorado in 1995 and her B.S. in Aerospace Engineering from the University of Alabama in 1993.

Penina Axelrad is Associate Professor of Aerospace Engineering Sciences with the Colorado Center for Astrodynamics Research at CU. Her research focuses on space applications of GPS and algorithms for GPS error mitigation. She received her Ph.D. from Stanford University in 1991 and her S.M. and S.B. from M.I.T.

ABSTRACT

A process was developed to use the GPS signal to noise ratio (SNR) to identify an effective reflector for a given antenna. This is termed an effective reflector because the reflector identified can account for a number of effects found in the signal, including such things as multiple reflectors, changes in reflectivity, and changes in signal phase upon reflection. A physical location is used simply as a means to represent the spatial correlation of the multipath. Once a effective reflector location has been found, a carrier phase correction profile is computed for that reflector. The measured carrier phase is then corrected by that amount and a new attitude solution is computed.

Using this technique, results from ground tests show that the RMS differential phase residuals improved from 11.37 mm to 8.56 mm, corresponding to a 25% improvement. These results were found using only a batch estimator to identify an effective reflector. For the CRISTA-SPAS flight data the lack of knowledge of the antenna gain pattern limited the ability of the method to determine a reliable reflector solution. Some residual improvement was found for the data. One such pass had a residual improvement from 6.4 mm to 5.5 mm. However, for much of the data, an effective reflector that improved the phase residuals could not be identified.

INTRODUCTION

High precision GPS applications such as attitude determination, static and kinematic survey utilize carrier phase data from two or more GPS antennas and receivers. While this technique is very effective in getting results at the several centimeter level, the factor limiting accuracy for short antenna separations is often multipath.

Much work has been done in the area of GPS multipath identification and correction. One approach is to correct for multipath within the receiver, as opposed to a post-processing technique. A few of the proposed internal receiver techniques include narrow correlators [Van Dierendonck, et al., 1992], edge correlators, and the multipath estimating delay lock loop (MEDLL) [Townsend, et al., 1995]. These methods can potentially reduce the amount of multipath in the observable at the expense of increased receiver complexity.

Another approach is to model the multipath for a specific antenna and environment using the geometrical theory of diffraction (GTD) [Hajj, 1990 and Lippencott, et al., 1993]. This approach requires a knowledge of the antenna gain pattern and the geometry and reflectivity of objects surrounding the antenna. Based on this information, a ray tracing algorithm determines a model of the resulting phase and amplitude of the multipath error. Corrections on the carrier have been confirmed by experimental results [Gomez, et al., 1995 and Irish, et al., 1998].

A method for post-processing of the GPS carrier phase signal using a procedure based upon the spatial correlation characteristics of multipath was first proposed by Cohen and Parkinson [1991]. Experimental data

collected on a fixed ground structure over the course of several days is used to create a map of multipath as a function of the direction of the incoming direct GPS signal. Based on the known attitude and baseline locations of the ground platform, carrier phase residuals are computed and prefiltered to remove receiver noise. Then, an eighth order spherical harmonic model is fit to the residuals as a function of azimuth and elevation of the incoming signals. Reductions of the residuals from 5.2 to 3.2 millimeters were shown by Cohen and Parkinson [1991] using this approach.

Another method for the post-processing the GPS carrier phase was implemented by Comp [1996]. Instead of modeling multipath in the residual phase, this approach utilizes the signal to noise ratio (SNR) in order to mitigate multipath. One advantage of using the SNR over the residual differential phase, as implemented by Cohen and Parkinson [1991], is that the SNR is much less sensitive to attitude errors than the residual differential phase, which is directly dependent on any errors in the attitude. The previous SNR method analyzes the data for individual satellite passes as a function of time, identifying individual frequency components in the signal due to multipath. Although this approach showed significant reduction in the phase multipath errors, it is not entirely effective for real-time applications because of the long convergence time required.

Ray, et al. [1998] developed a method to reduce multipath by using a system of multiple, closely spaced antennas in a static multipath environment. With the location of the antennas precisely known, it is possible to isolate the direct signal phase and discard the portion of the signal corrupted by multipath. A drawback of this system is that it relies on using the phase measurement, which is highly sensitive to errors in antenna location and attitude. Also, it relies on using a number of closely spaced antennas. Although it may be possible to do this for some ground stations, it would be too costly to use in a spacecraft environment for attitude applications.

The purpose of this research is to avoid the approaches that increase the cost or complexity of an experiment by altering the receiver architecture or including additional antennas. A method will be implemented in which post-processing data from any type of receiver-antenna setup can be used. Additionally, the GPS SNR measurement is desirable for use in a post-processing technique, as was used in the research by Comp [1996], because the SNR is less sensitive than the phase residuals to errors in the attitude and baseline solutions.

This paper discusses a method by which to reduce the multipath in the carrier phase by utilizing the spatially correlated characteristics of multipath, as viewed in both the GPS carrier phase and SNR. The spatial dependence of multipath is characterized by an effective reflector location and corresponding multipath signal amplitude. Therefore, when an effective reflector is determined for a set of SNR data at some time from a certain portion of the sky, the same reflector can be used for data at a later point in time if the originating signal passes through the same region of the sky. The location and amplitude of the effective reflector are in turn used to generate corrections in the carrier phase that are caused by the effective reflector.

In the next section a discussion of carrier phase multipath is given, followed by the methodology behind the reflector identification algorithm. Finally, results are presented for static ground data and for flight data from the CRISTA-SPAS spacecraft.

BACKGROUND

Multipath occurs when an electromagnetic signal arrives at an antenna, not along a direct path, but via one of the multiple paths the signal takes as it reflects off an object near an antenna. Multipath may either be diffuse or specular in nature. In contrast to the correlated nature of specular multipath, diffuse multipath takes on an unbiased, random appearance, and is removed more easily in filtering than specular multipath. Therefore, only specular multipath will be considered in this research.

Path Delay

When a signal enters the antenna via an indirect route, the extra distance the signal travels as compared to a direct line of sight to the satellite is defined as path delay. For the purposes of this study, we model only a perfectly conducting planar reflector, for which the angle of reflection is equal to the angle of incidence.

The path delay due to a planar reflector is illustrated in Figure 1. In this figure, $\hat{n}$ is the normal vector of the plane, d is the normal distance from the plane reflector to the antenna, and $\hat{e}$ is the unit line of sight vector from the user to the GPS satellite. The physical path delay is shown in the figure as the bold part of the reflected signal. An expression for the path delay, ψ, is given in equation (1). Note in equation (1) that the path delay is only modeled as a function of the distance of the reflector from the antenna (d), the orientation of the reflector ($\hat{n}$), and the direction of the line of sight vector ($\hat{e}$), thus making it a purely spatially correlated phenomenon.
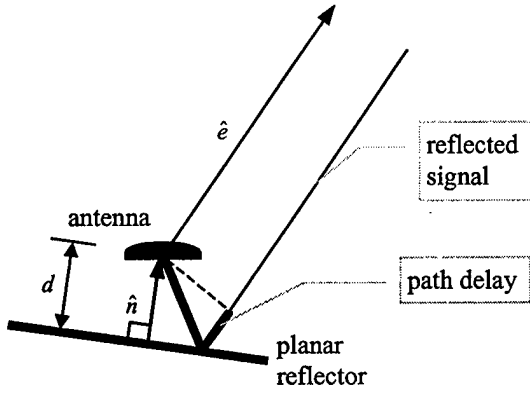
Figure 1: Path Delay for a Reflected Signal

$$\psi = 2d(\hat{e}\cdot\hat{n}) \qquad (1)$$

Multipath in the GPS SNR and Differential Phase

The path delay due to a reflector is identifiable in three measurements from a GPS receiver – the pseudorange, the carrier phase and the SNR. Here we focus on the latter two measurements depicted in the phasor diagram shown in Figure 2. The amplitude values, denoted by A, correspond to SNR measurements and the angular values, denoted by ϕ, correspond to phase measurements. In this figure A_c is the composite SNR measurement and ϕ_c is the composite carrier phase. These are the quantities that the receiver measures. In addition to the composite signal phasor, two others are represented in this figure – the direct signal phasor and the multipath phasor.
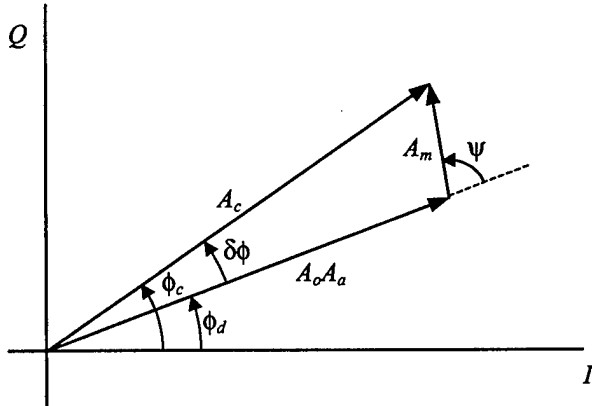

Figure 2: GPS Signal Phasor Diagram

The direct signal SNR amplitude is A_aA_o, where A_a is the normalized antenna gain and A_o is the constant part of the direct signal amplitude. The multipath amplitude is A_m and the path delay, ψ, is the phase of the multipath relative to the direct signal. Using the law of cosines, the equation for the composite SNR in terms of the direct and multipath signals is shown in equation (2).

$$A_c^2 = (A_oA_a)^2 + A_m^2 + 2A_oA_aA_m\cos\psi \qquad (2)$$

The composite carrier phase measurement, ϕ_c, is also a function of the multipath amplitude and phase. The phase due to multipath is the residual phase, $\delta\phi$. The residual phase is represented using equation (3).

$$\tan(\delta\phi) = \frac{A_m\sin\psi}{A_oA_a + A_m\cos\psi} \qquad (3)$$

In order to gain a better understanding of the dynamics of this problem note that as a GPS satellite passes overhead, the relationship between the line of sight vector and the vector normal to the plane will change, causing the path delay to change. As the path delay increases or decreases, the multipath phasor rotates about the end point of the direct phasor. This in turn causes the composite SNR and carrier phase magnitudes to oscillate sinusoidally as the path delay either increases or decreases, thus creating the correlated error found in the two signals.

Reflector Identification Algorithm

A batch estimation filter is implemented in order to identify an effective reflector location. The batch algorithm utilizes the dependence on the reflector location in the path delay equation. In this evaluation, the square of the SNR for a single satellite pass is used as the measurement. The squared value is used so that the representation for SNR in equation (2) can be used directly.

A model for the antenna gain is needed in order to use the SNR for reflector identification. The line of sight vectors are rotated from the local frame into the antenna frame using an initial estimate for the spacecraft local-to-body attitude. Given the line of sight vectors in the antenna frame, the azimuth and elevation of the GPS signal relative to the antenna is determined, and thus the antenna gain for that satellite pass can be found.

The state vector for the batch filter is:

$$x = \begin{bmatrix} d & az & el & A_o & A_m \end{bmatrix} \qquad (4)$$

The state is composed of five variables, where d is the distance to the reflector, az and el are the azimuth and elevation of the plane normal vector, A_o is the constant part of the direct signal amplitude in amplitude units, and A_m is the multipath amplitude in amplitude units. The azimuth and elevation of the reflector are related to the plane unit normal vector by the following equation:

$$\hat{n} = \begin{bmatrix} \sin(el) & \cos(el)\cos(az) & \cos(el)\sin(el) \end{bmatrix}, \qquad (5)$$

where an elevation angle of 90 degrees is defined to be in the positive x-direction and an azimuth of zero degrees is in the positive y-direction.

Before the batch estimation algorithm can be performed on the SNR measurement data, the state variables must be initialized. This initialization is done by searching over a coarse three-dimensional grid containing values of distance, azimuth, and elevation, representing the full range of possible reflector locations. For each of these assumed locations and the GPS lines of sight for the satellite pass, a path delay profile is computed, using equation (1). Note that if the line of sight vector drops below the planar reflector, the path delay is set to zero and no multipath is considered for this region. Additionally, an estimate for the constant part of the direct signal, A_o, is computed by performing a least squares fit to the SNR data as shown in equation (5).

$$SNR \approx A_o A_a \qquad (5)$$

Once the path delay and direct signal strength are known, an estimate of the multipath amplitude, A_m, is computed by solving equation (2) using least squares, where the composite amplitude is the measured SNR. After trying each of the possible reflector locations and computing the corresponding direct and multipath amplitudes, the location and amplitudes with the lowest SNR residual is used to initialize the batch algorithm.

After an initial estimate for the state is found, the batch estimator is run. The measurement sensitivity is computed by taking partials of the measurement equation, defined in equation (2), with respect to the state variables. The measurement partial matrix, $\mathbf{H}$, is defined by:

$$\left[\frac{\partial(A_c^2)}{\partial d} \quad \frac{\partial(A_c^2)}{\partial az} \quad \frac{\partial(A_c^2)}{\partial el} \quad \frac{\partial(A_c^2)}{\partial A_o} \quad \frac{\partial(A_c^2)}{\partial A_m} \right] \qquad (6)$$

$$\frac{\partial(A_c^2)}{\partial d} = -4 A_m A_o A_a (\hat{e} \cdot \hat{n}) \sin\psi$$

$$\frac{\partial(A_c^2)}{\partial az} = -4 A_m A_o A_a d \left(-e_y \cos el \sin az + e_z \cos el \cos az \right) \sin\psi$$

$$\frac{\partial(A_c^2)}{\partial el} = -4 A_m A_o A_a d \left(e_x \cos el - e_y \sin el \cos az - e_z \sin el \sin az \right) \sin\psi$$

$$\frac{\partial(A_c^2)}{\partial A_o} = 2 A_o A_a^2 + 2 A_m A_a \cos\psi$$

$$\frac{\partial(A_c^2)}{\partial A_o} = 2 A_m + 2 A_o A_a \cos\psi$$

The measurement residual is the difference between the measured SNR^2 and that predicted from (2) using the initial estimate of the state. The update to the state, $\hat{x}$, is computed in a least squares sense using the measurement partial matrix and the measurement residual, y, as shown in equation (7).

$$\mathbf{H}^T \mathbf{H} \hat{x} = \mathbf{H}^T y \qquad (7)$$

After an update to the state is computed, it is added to the current estimate of the state, and this process continues until the state estimate converges.

With the computed state vector for each antenna, carrier phase corrections are computed using equation (3) for each satellite pass in which a reflector is identified. The differential phase correction is computed by differencing the corrections for the individual antennas. The differential phase corrections are then subtracted from the measured values and the updated differential phase measurements are filtered using an attitude estimation algorithm developed by Ward [Ward, 1996].

The performance of this algorithm is tested by comparing the phase residuals before and after the corrections for an effective reflector has been applied. For flight data, in addition to comparing the residuals, the resulting improvement in the attitude solution will be noted.

RESULTS

Simulations

To aid in the development of this approach, multipath data were simulated using the Ohio State Basic Scattering Code. These simulations were used to study multipath in simple reflecting environments using ideal antennas. The data generated included a single large planar reflector and only specular reflection was considered. This was done primarily as a tool to test the theory behind the reflector identification method. The data were simulated and both SNR and carrier phase measurements were produced. The simulated measurements were shown to be the same as data calculated using models presented previously for the same reflector location and multipath amplitude. The data were processed for a single antenna using the reflector identification algorithm and the reflector and amplitudes were accurately found.

Ground Tests

In order to test the algorithm in real applications, data collected by C. Behre at the Naval Research Laboratory test facility on October 7, 1995 were processed. A Trimble TANS Vector attitude receiver was used for the testing [Cohen, 1992], [Trimble, 1993]. Three Trimble patch antennas, a master and number 1 and 3 slaves, were affixed to a JAWSAT satellite mockup mounted upon a three-axis rotational spin table. The antenna height was approximately 1.5 meters above a concrete surface. Additionally, a 0.6 by 0.6 square aluminum plate reflector, inclined at 45 degrees was mounted to the corner in which the number 2 slave would normally be affixed. During the experiment, 90 minutes of static data were collected. Upon evaluation the data were found to show very clear signs of multipath, both in the carrier

phase and in the SNR. A photograph of the experimental setup is shown in Figure 3.
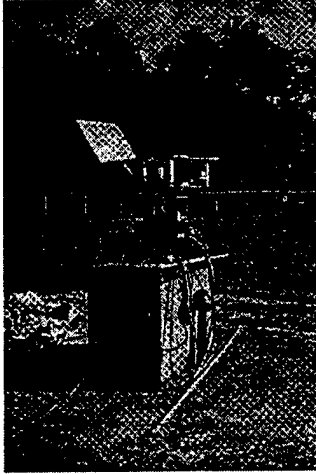

Figure 3: Ground test experimental setup

A satellite pass of GPS PRN 17, lasting approximately one hour was chosen for evaluation. The reflector identification algorithm is implemented using the raw SNR data and the antenna gain data for the Trimble patch antenna. Upon implementation of the batch estimator, it was found that the state variables corresponding to the azimuth and elevation of the plate are not observable for a single satellite pass of data. Therefore, the azimuth and elevation found during the initialization processed were held fixed during the batch process, while the distance to the reflector and the direct and multipath amplitudes were estimated. After implementation of the batch estimator, the reflector identified has the state shown in Table 1.

Table 1: Reflector locations for ground test data

ant	d (m)	az (°)	el (°)	A_o (AMU)	A_m (AMU)
m	1.790	2.7	81.7	31.059	1.472
1	1.837	9.0	86.1	22.964	2.214
3	1.867	92.8	68.1	20.927	0.819

Figures 4-6 show the measured and computed SNR^2 for the three antennas for the states in Table 1. The improvement in the residual phase using these reflectors is shown in Figures 7 and 8. Upon applying this correction to the phase for the entire pass, the RMS of the residuals for baseline 1 reduces from 11.37 mm to 8.56 mm, corresponding to a 25% error reduction. The RMS of the residuals for baseline 3 changes only slightly from 29.27 mm to 29.08 mm.
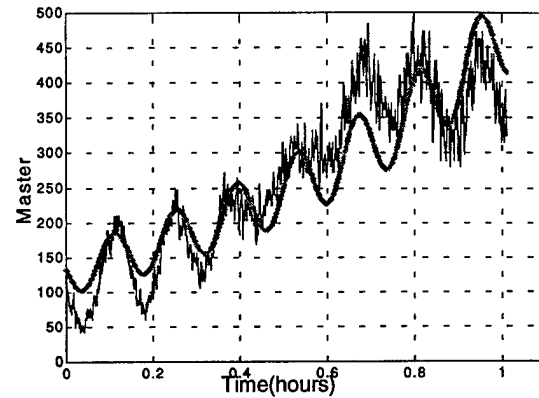

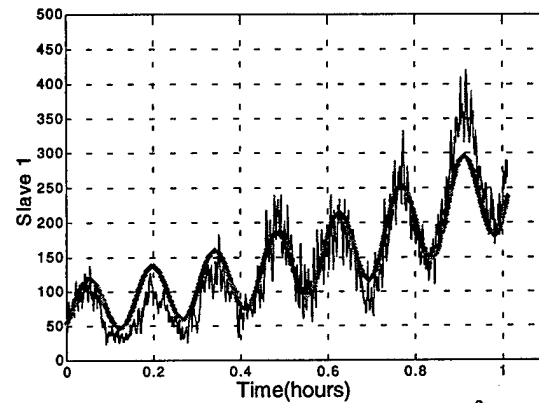Figure 4: Measured (blue) and computed SNR^2 (green) for the master antenna

Figure 5: Measured (blue) and computed SNR^2 (green) for the number one slave antenna
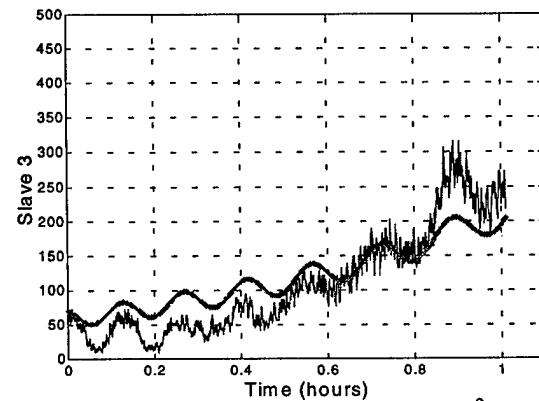

Figure 6: Measured (blue) and computed SNR^2 (green) for the number three slave antenna
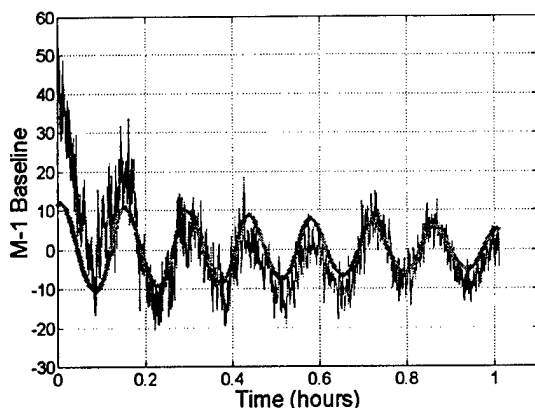
Figure 7: Residual differential phase (blue) and computed phase corrections (green) for baseline 1
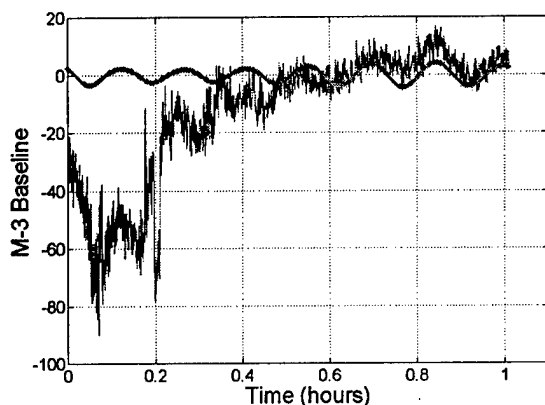

Figure 8: Residual differential phase (blue) and computed phase corrections (green) for baseline 3

For these ground test data, the method works very well in identifying an effective reflector by which to model multipath. The ground was identified as the primary source of multipath. The sources of error for the results shown in Figures 7 and 8 are believed to be caused by two things. First, the multipath amplitude is being modeled as a constant value. An adaptive means by which to estimate the multipath amplitude would improve these results, since it is clear in both the SNR and phase plots that the multipath amplitude does vary. Additionally, there is a lower frequency oscillation in the master and the number 3 slave antennas that is not being accurately modeled by the single large reflector approximately 1.75 meters away. Estimation of a second effective reflector, which is possibly the square aluminum plate, would likely also decrease the differential phase residuals.

CRISTA-SPAS

The Space Shuttle Atlantis deployed the CRISTA-SPAS satellite on November 3, 1994. A photograph of the satellite being released is shown in Figure 9. During its 11-day mission, it remained within a few kilometers of the Shuttle, with the primary purpose of the mission being

observation of the Earth's middle atmosphere. Three-axis control of the spacecraft was required in order to point a telescope at an area 62.9 kilometers above the WGS-84 ellipsoid. A star tracker-gyro inertial reference unit (IRU) provided attitude information for closed loop control and an Alcatel GPS receiver provided position information [Brock, et al, 1995].
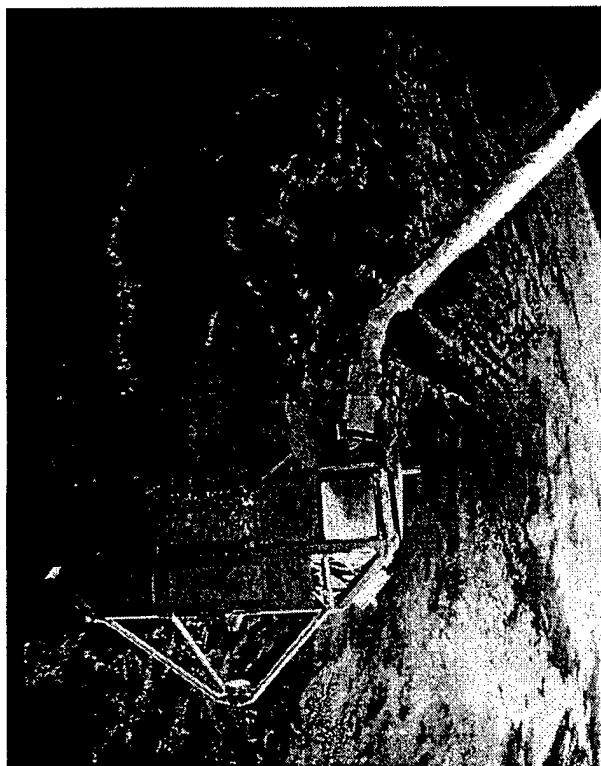

Figure 9: Photograph of CRISTA-SPAS (Courtesy J. Rodden, Loral Space Systems)

Before the CRISTA-SPAS data are processed using the reflector identification method, the spatial repeatability of the data is tested. This is done by identifying four GPS tracks that follow the same path. The azimuth and elevation of the four tracks are shown in Figure 10. The SNR and residual differential phase for these satellite passes are shown in Figures 11 and 12, respectively.
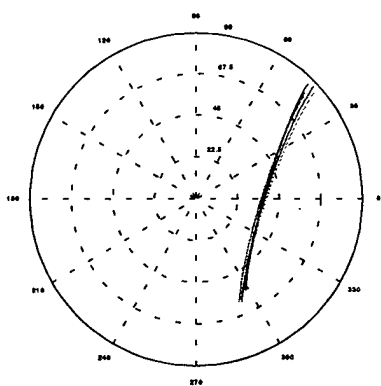
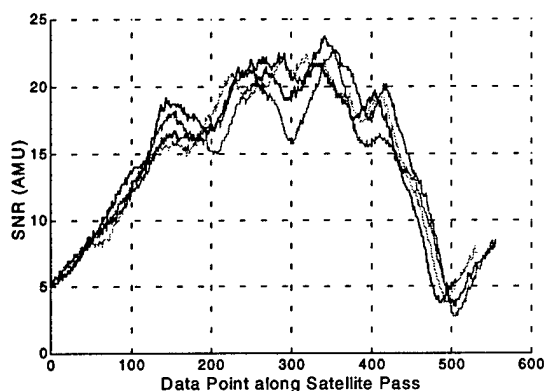Figure 10: 4 satellite passes following similar tracks

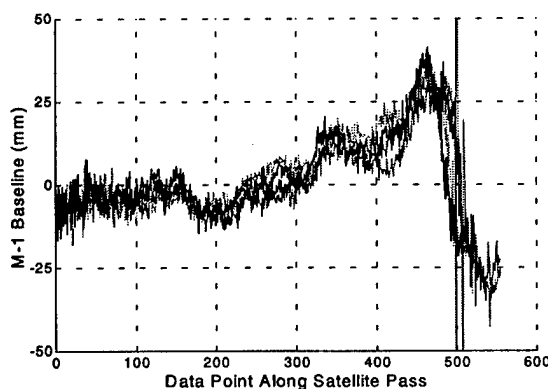Figure 11: SNR for the Slave 3 antenna for the 4 passes

Figure 12: Residual differential phase for baseline 1 for the 4 passes

Since both the SNR and residual phase follow the same trends for the similar satellite passes, it can be inferred that the data are highly spatially correlated. It is reasonable, therefore, to assume that the reflector identification method will be effective in isolating an effective reflector location that will reduce the phase residuals for not only a single pass, but other passes that follow the same path in the sky. Also, once an effective reflector has been found for that portion of the sky, there is no need to re-solve for a new location. The previous computed residuals may simply be applied or the reflector

location may be iterated upon by using the previous reflector location as the *a priori* state.

Another test of the repeatability of phase multipath was conducted by implementing a phase map correction. A detailed explanation of the process and results are shown in [Axelrad and Reichert, 1997]. This involves computing phase residuals for all 32 hours of satellite data and generating a phase correction map as a function of the line of sight vector. This is based on the method presented in [Cohen and Parkinson, 1991]. In this evaluation, a number of methods were used to implement a fit to the data, including a spherical harmonic fit, a polynomial fit, and a correction grid method. The correction grid fit was shown to provide the best fit to the phase residuals.

The correction grid is generated by sorting the data into bins based on azimuth and elevation values of the incoming signal. The correction value for each grid point is set to the mean value of all the residuals within each bin. The grid computed has a rectangular resolution of approximately 1 deg × 1 deg and is shown for baseline one in Figure 13. The correction grid may either be applied as either a table look-up or it may be interpolated. Upon implementation of the correction grid to the phase data using interpolation, the RMS of the residuals were reduced by 51%, 52%, and 41% for baselines 1, 2, and 3, respectively. A linearized Kalman filter is implemented using the improved phase measurements. The resulting attitude error improves from 0.12 to 0.05 degrees in yaw, 0.10 to 0.04 degrees in roll and 0.20 to 0.14 degrees in pitch.
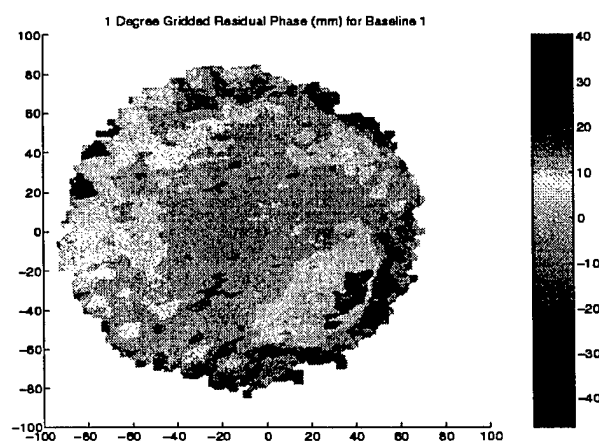

Figure 13: Phase correction grid map for Baseline 1

This method of computing corrections to the phase, using the attitude solution is somewhat flawed because it requires ideal attitude and baseline solutions in order to accurately determine the phase residuals. Any error in the attitude or baselines directly maps into the computation for the residual phase. Therefore it is difficult to separate errors in attitude from multipath. In order to avoid the

problem a dependence on SNR, rather than phase, is utilized because the SNR is much less sensitive to attitude errors.

Utilizing the SNR, the reflector identification algorithm is implemented for the CRISTA-SPAS data. The gain pattern used for the ground tests for the Trimble patch antennas did not match well with the received SNR values. Therefore a simple two-dimensional polynomial fit to the SNR data was used for the antenna gain value, A_a.

The reflector identification method was implemented for a number of satellite passes. The SNR fits for the four antennas for a single pass of satellite PRN 1 are shown in Figures 14 – 17. One successful pass is for the off-baseline formed by the number 2 and 3 slave antennas. The phase correction for this off-baseline is shown in Figure 18. Unfortunately, an appropriate effective reflector was not located for the master antenna, as is represented by the phase residual for baseline 1 shown in Figure 19, so the phase measurements could not be adequately updated for this satellite pass.
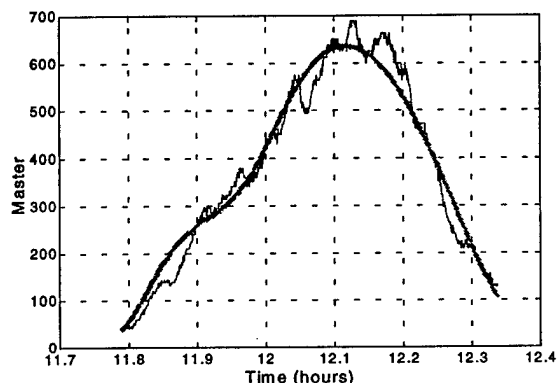

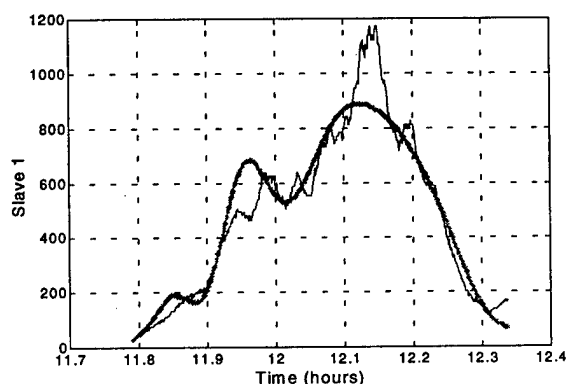Figure 14: Measured (blue) and computed (green) SNR^2 fit for the Master antenna

Figure 15: Measured (blue) and computed (green) SNR^2 fit for the Slave 1 antenna
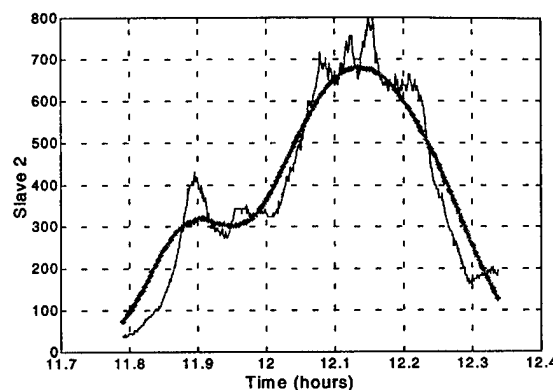

Figure 16: Measured (blue) and computed (green) SNR^2 fit for the Slave 2 antenna
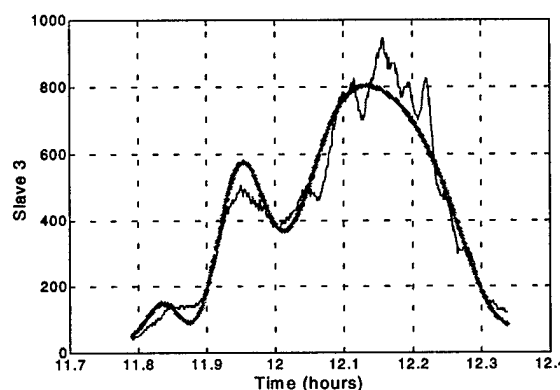

Figure 17: Measured (blue) and computed (green) SNR^2 fit for the Slave 3 antenna
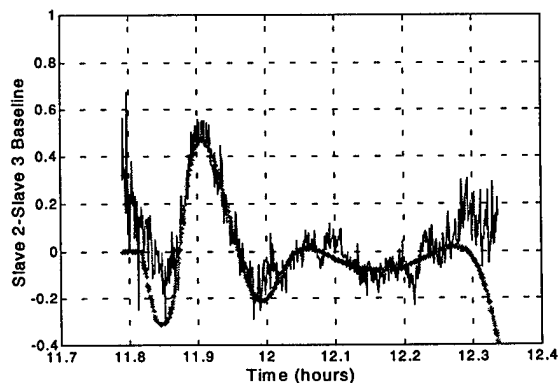

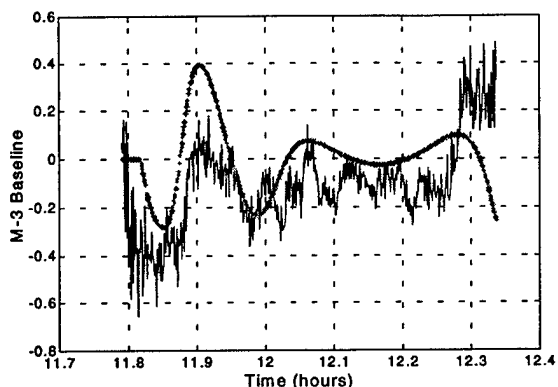Figure 18: Residual fit for the Slave 2-Slave 3 off-baseline

Figure 19: Residual fit for baseline 3

Tables 2 and 3 list results for three baselines for PRN 1, baseline 2 and PRN 25, baselines 1 and 2, 1 in which the residuals are improved. Table 2 includes the reflector location and the multipath amplitude and Table 3 shows the residual differential phase before and after the phase corrections are applied. For these satellite/baseline combinations in which phase residuals were improved, the phases measurements were corrected and an attitude point solution was recomputed using the algorithm developed by Ward [Ward, 1996]. Because only a total of three baselines were corrected with minimal phase improvements, no appreciable attitude improvement was found.

Table 2: Reflector location and amplitude for CRISTA-SPAS data

PRN	antenna	d (m)	az (deg)	el (deg)	A_m (AMU)
1	master	.078	285	75	2.45
1	slave 2	.079	240	72	3.84
25	master	.428	220	80	0.69
25	slave 1	.385	300	70	1.87
25	slave 2	.141	80	70	1.31

Table 3: Phase improvements for CRISTA-SPAS data

PRN	Baseline	residual before	residual after
1	m-2	7.5095	7.3611
25	m-1	6.4085	5.5335
25	m-2	6.7899	6.4252

CONCLUSIONS AND FUTURE WORK

In this paper a method to reduce carrier phase multipath by identifying an effective reflector using the GPS SNR measurement was presented. The method utilizes the known spatial correlation of multipath to identify a reflector location and direct signal and multipath amplitudes.

The results shown for the ground data indicate significant improvement to the residual differential phase using only a single reflector and multipath amplitude identified from a batch estimation scheme. It is likely that more improvement would result if the multipath amplitude were to be adaptively estimated over time to better account for the changing reflectivity of the reflecting surface. The results found by implementing the method for the CRISTA-SPAS flight data indicate some potential to identify a reflector capable of reducing carrier phase multipath. However, these data demonstrated that the ability to identify a reflector from SNR data is limited by the poor knowledge of the antenna gain pattern.

In future work the batch filter will be replaced by an adaptive filter which will allow the reflector location and multipath amplitude to slowly change as the satellite passes overhead. Additionally, a second reflector will be identified in some situations where it is clear that both high and low frequency multipath components exist, being caused by reflectors both far from and near to the antenna.

ACKNOWLEDGEMENTS

REFERENCES

[Axelrad and Reichert, 1997] Axelrad, P. and Reichert, A., "Algorithms for Calibration of Multipath Errors Using Micro-Mechanical Gyros," Draper Lab IR&D Project No. 802, Final Report, July 1997.

[Brock, et al., 1995] Brock, J. K., Fuller, R., Kemper, B., Mleczko, D., Rodden, J., Tadros, A., "GPS Attitude Determination and Navigation Flight Experiment," ION GPS-95, Palm Springs, CA, September 1995, pp. 545-554.

[Cohen and Parkinson, 1991] Cohen, C. E. and Parkinson, B. W., "Mitigating Multipath in GPS-Based Attitude Determination," *Advances in the Astronautical Sciences*, AAS Guidance and Control Conference, Keystone, CO, Vol. 74, Univelt, San Diego, 1991.

[Cohen, 1992] Cohen, C. E., *Attitude Determination Using GPS*, Ph.D. Dissertation, Department of Aeronautics and Astronautics, Stanford University, December 1992.

[Comp, 1996] Comp, C. J., *GPS Carrier Phase Multipath Characterization and Mitigation Technique Using the Signal-to-Noise Ratio*, Ph.D. Dissertation, Department of Aerospace Engineering Sciences, University of Colorado, July 1996.

[Gomez and Hwu] Gomez, S. F., Hwu, S., "Comparison of Space Shuttle GPS Flight Data to Geometric Theory of Diffraction Predictions", ION GPS-97, Kansas City, MO, September 1997.

[Hajj, 1990] Hajj, G. A., "The Multipath Simulator: A Tool Toward Controlling Multipath," *Proceedings of the 2nd Symposium on GPS Applications in Space*, Hanscom AFB, MA, February 1990.

[Irish, et al., 1998] Irish, K. J. , Gold, K., Born, G., Markin, R., Reichert, A., Binning, P., Axelrad, P., and Behre, C., "Precision Orbit Determination for GFO and GFO-2, *Journal of Spacecraft and Rockets*, Vol. 35, no. 3, May-June 1998.

[Lippencott, et al., 1993] Lippencott, W. L., Milligan, T., and Igli, D. A., "Method for Calculating Multipath Environment and Impact on GPS Receiver Solutions Accuracy," ION National Technical Meeting, San Francisco, CA, January 1993.

[Ray, et al., 1998] Ray, J. K., Cannon, M. E., Fenton, P., "Mitigation of Static Carrier Phase Multipath Effects Using Multiple Closely-Spaced Antennas," ION GPS-98, Nashville, TN, September 1998.

[Townsend et al., 1995] Townsend, B. R., Fenton, P. C., Van Dierendonck, K. J., and Van Nee, D. J. R., "Performance Evaluation of the Multipath Estimating Delay Lock Loop," *Navigation*, Journal of the ION, Vol. 42, No. 3, Fall 1995, pp. 503-514.

[Trimble, 1993] *TANS Vector Specification and User's Manual*, Trimble Navigation Limited, June 1993.

[Van Dierendonck, et al., 1992], Van Dierendonck, A. J., Fenton, P., Ford, T., "Theory and Performance of a Narrow Correlator Spacing in a GPS receiver," *Navigation*, Journal of the ION, Vol. 39, No. 3, Fall, 1992, pp. 265-283.

[Ward, 1996] Ward, L. M., *Spacecraft Attitude Estimation Using GPS: Methodology and Results*, Ph.D. Dissertation, Department of Aerospace Engineering Sciences, University of Colorado, July 1996.

Proposal for Precise Satellite-to-Satellite Relative Navigation and Time Transfer Using GPS

Dolan Highsmith

October 15, 1999

Contents

Chapter 1

Introduction

Accurate relative navigation of spacecraft permits capabilities such as rendezvous and formation flying—key aspects of many current and future space missions. In low earth orbit (LEO), such missions can use the Global Positioning System (GPS) signal for relative positioning and data time-tagging. However, little has been published on the natural extension to GPS relative navigation: precise time and frequency transfer on orbit. In terrestrial time keeping, GPS is widely used for nanosecond- and even picosecond-level time transfer, given long averaging times and accurate knowledge of positions and GPS signal error sources. My proposed research will investigate methods for extending GPS time transfer to satellite-to-satellite applications at the five nanosecond level or better in near real time. The primary topic is determination and demonstration of algorithms for precise relative position, velocity, and GPS receiver clock bias and frequency through use of both GPS code and carrier phase measurements. The algorithms will be tested using flight data and hardware-in-the-loop simulation data. This report discusses the progress to date and the steps proposed to reach the stated goals.

1.1   Previous Research

1.1.1   GPS Relative Navigation

Recent years have seen an abundance of GPS relative navigation research. An extensive evaluation of satellite-to-satellite GPS relative navigation algorithms is presented by Binning [1]. He generates data for two co-orbiting satellites in LEO using both software and hardware-in-the-loop simulations and presents the results for four separate algorithms. Two of his methods compute the relative state by subtracting absolute orbit estimates determined using GPS P-code pseudorange observations, while the two other methods explicitly estimate the relative state. The first method generates independent orbit estimates of each vehicle using all the GPS satellites in view to the respective receivers, achieving a relative position accuracy of about 1 m. A more complex method interpolates the pseudorange observations from the two receivers to a common time and solves for the absolute orbits using only common-view satellites. An extension to this method uses single difference pseudoranges to estimate the relative state directly, while also estimating the absolute state of one of the vehicles as before. These two common-view techniques achieve relative position accuracies of approximately 15-25 cm. Finally, Binning presents an algorithm which uses both GPS transmission frequencies to create a widelane carrier phase observation. Using single differences with this type of observation increases accuracy to approximately 3 cm in relative position. It should be noted that Binning did not use a more accurate external reference clock during the hardware simulations, so the accuracy of his clock bias and frequency estimates are not known.

Additional simulation work has been performed by Upadhyay et al. [2] in support of automated rendezvous and docking studies for NASA. Their two-stage GPS relative navigation scheme consists of a meter-level filter and a centimeter-level filter. The meter-level filter generates smoothed absolute and relative orbit estimates for two vehicles using GPS pseudorange and either Doppler or range-rate. The centimeter-level filter refines the relative state estimates by solving for the

double-differenced carrier phase ambiguities. Hardware-in-the-loop tests for the meter-level filter produces RSS relative position and velocity errors of 0.887 m and 0.8 cm/s, respectively. Results from software simulated data on the centimeter-level filter show relative RSS accuracies of 0.11 m in position and 1 cm/s in velocity.

Cox and Brading [3] also developed a GPS relative navigation filter that resolves the carrier phase ambiguities. In their paper, they discuss implementation of the LAMBDA method for ambiguity resolution in an optimal Kalman filter and evaluate its performance on simulated data. The measurement types used are single-frequency, uncorrupted P-code and double-differenced accumulated phase. For the 10-km baseline case, the relative radial position errors are generally less than 2 cm. Increasing the baseline to 100 km results in radial position errors of approximately 3-10 cm.

Two notable flight experiments utilizing GPS for relative navigation occurred with the NASA STS-80 Shuttle mission and the NASDA ETS-VII flight experiment. Schiesser et al. [4] present results from the Shuttle/ORFEUS-SPAS free-flyer rendezvous during the STS-80 mission in December 1996. Their filter uses GPS coarse/acquisition (C/A) code pseudoranges to solve for the absolute orbits of the two vehicles, then differences them to form the relative orbit. The filter is designed to processes asynchronous observations from the two receivers in real time, accepting input from the Shuttle IMU for maneuver compensation. A unique element of this filter is that it uses the same filter-estimated range bias state and covariance matrix elements for both vehicles when processing observations from common-view GPS satellites. Given the highly dynamic environment during rendezvous, the filter obtained RSS relative position and velocity errors of 9 m and 12.6 cm/s, respectively.

Most recently, D'Souza et al. [5] from Draper Lab developed a filter for validation of algorithms for use with two NASDA projects, Engineering Test Satellite 7 (ETS-VII) and the H-II Transfer Vehicle (HTV). The filter estimates explicitly the relative position, velocity, and GPS receiver clock bias and frequency using single difference C/A code pseudoranges. The asynchronous pseudoranges

from one receiver are linearly interpolated to the times of the other to allow measurement differencing. Excellent simulation results were obtained. Presuming NASDA implemented this filter for ETS-VII, Mokuno et al. [6] indicate that on-orbit results were also good, obtaining a GPS-derived relative range within 1 m of the rendezvous radar measurement and an in-plane velocity error within 2 cm/s.

As for GPS relative navigation combined with time transfer for orbiting platforms, very few references appear in the literature. Cox and Brading have published two such papers [7, 8]. In the most recent of the two (1997), they use software simulated orbits with baselines of 100 km and 10 km separating the two vehicles. (The same simulation is used for their subsequent paper using the LAMBDA method [3], but there is no mention of time transfer in that paper.) Dual-frequency, uncorrupted P(Y) code and carrier measurements are provided by the simulation. The filter creates differences and sums of pseudoranges and differences of accumulated phase measurements to use as filter observations. The filter estimates absolute position, velocity, clock time error, and clock frequency error for each vehicle (16 states), as well as floating-point single-difference carrier phase ambiguities for each common-view GPS satellite. At 100 km, the relative RMS accuracies are given as 7 cm in position, 0.01 cm/s in velocity, 0.4 ns in time (ignoring common-mode errors), and 7×10^{-12} in fractional frequency. Note, however, that the simulation employs a second-order stochastic model to generate the true receiver clock errors, and that the second-order clock model in the filter uses the same parameters as the truth for propagating clock errors. Hardware-in-the-loop simulations do not have the benefit of setting or knowing precisely the clock behavior.

1.1.2 GPS Time Transfer

Although not much has been published on GPS time transfer in orbit, extensive research has been performed on terrestrial applications of GPS time transfer. Indeed, use of GPS is currently the foremost method for precise time and time interval distribution. Detailed summaries of precise

timing using GPS can be found in [9, 10, 11]. Allan and Weiss first proposed the now standard GPS common-view (CV) technique, which involves differencing C/A code pseudorange observations from different timing sites with known locations [12]. Current multi-channel CV results by Levine indicate a 3-5 ns RMS accuracy [13]. Larson and Levine further refine time transfer accuracies by employing the GPS carrier phase, achieving a stability of 100 ps and frequency uncertainty of 2 parts in 10^{15} for 1 day averages [14].

On-orbit time transfer will not have the benefit of extremely precise knowledge of the antenna locations, as in most terrestrial time transfer applications. Error sources must be treated differently in orbit, and the averaging times must be shorter for meaningful application in real time. However, picosecond accuracies are not required for the on-orbit application. Thus, a combination of precise relative navigation and time transfer techniques is sought.

1.2 Contributions

The primary contribution of this research will be the ability to synchronize the clocks of a pair of orbiting satellites in real time to five nanoseconds with respect to each other. Previous research has shown precise relative navigation of satellites and, separately, precise time and frequency transfer using GPS. However, none has shown precise relative navigation and timing of satellites in orbit in real time using actual hardware data.

Another contribution of this research is the development of a time transfer test bed for performing hardware simulations of multiple satellites. This research is being performed at the Naval Research Laboratory, which is uniquely equipped for such a test bed. Details given in a later section show that the test bed will measure the absolute and relative clock behavior of the hardware, providing a truth for comparison. Thus, the relative timing algorithms can be designed to reach an estimation accuracy equivalent to the measured precision of the hardware.

1.3   Overview of Report

Chapter 2 provides the details of the current version of the extended Kalman filter for relative navigation. Chapter 3 describes the flight experiment performed during a Shuttle mission and the results obtained with the current filter. Chapter 4 shows the performance of the filter on a data set which more closely resembles expected spacecraft dynamics and data quality. These data were obtained from a previous hardware simulation run by Binning in [1]. Finally, Chapter 5 details the proposed time transfer test bed and testing procedure.

Chapter 2

Relative State Kalman Filter

2.1 Overview

An extended Kalman filter that directly estimates the relative state between two co-orbiting ve-
hicles using single difference pseudorange observations has been developed. This filter is used in
conjunction with an existing GPS absolute orbit determination utility, which provides an estimate
of the absolute orbit of the passive vehicle to the relative filter. Use of single difference pseudoranges
reduces errors inherent in using GPS by removing common mode errors, such as the satellite clock
error. Furthermore, directly estimating a relative state allows the use of the Clohessy-Wiltshire
(CW) equations for state and error propagation. In fact, in its current form the relative filter
requires no integration.

Specifically, this filter estimates a relative position and velocity and relative receiver clock bias
and frequency. It uses the CW equations with velocity aiding to propagate the position and velocity,
incorporating the absolute orbit estimate of the passive vehicle to compute the mean motion. The
CW equations are also used to propagate the covariance. The measurement update computes the
observed and predicted single difference pseudoranges, where the predicted quantity accounts for

the body-fixed GPS antenna offset from the center of gravity by using a reported attitude estimate.

The relative state $\mathbf{s}_r$ is expressed by

$$\mathbf{s}_r = \begin{bmatrix} \mathbf{r}_r^T & \mathbf{v}_r^T & b_r & f_r \end{bmatrix}^T. \tag{2.1}$$

where $\mathbf{r}_r$ is position, $\mathbf{v}_r$ is velocity, b_r is clock bias, and f_r is frequency. The filter position and velocity coordinate frame is centered on one of the vehicles and expressed in radial, in-track, and cross-track (RIC) directions. The relative state is referenced to the passive vehicle in the case of a rendezvous. In the case of two non-thrusting vehicles, one is arbitrarily chosen to define the frame of reference. The covariance and process noise values are also specified in the RIC directions. This formulation permits more direct use of the CW equations for state and covariance propagation.

The Relative State Kalman Filter (RSKF) is designed to handle asynchronous GPS code pseudoranges from the two receivers, absolute orbit estimates for the passive vehicle, and GPS satellite position vectors. Since the RSKF is designed to work in tandem with an external GPS absolute orbit determination (AOD) utility, output from it is used as input to the RSKF. The external AOD program generates the absolute orbit estimates of the passive vehicle using GPS code pseudoranges and broadcast GPS satellite orbits. The orbit estimates, along with the GPS observations and satellite positions used to compute them, are output from the AOD program for use as input to the RSKF. Within the RSKF the active vehicle pseudoranges are interpolated to the times of the passive vehicle pseudoranges and positions.

Inertial-to-body attitude quaternions and delta-V vectors can also be input to the RSKF. The attitude quaternions are needed to account for the GPS antenna CG offsets, which are specified in a body-fixed frame. The inertial-to-RIC rotation is computed using the absolute position estimate of the passive vehicle. The delta-V vectors are used in the time update propagation to account for maneuvers above a specified threshold.

2.2 Time Update

As stated previously, the CW equations are used in this filter for relative state and covariance propagation. From Prussing and Conway [15], the CW equations in state transition matrix form are

$$\Phi_{\mathbf{r},\mathbf{v}}\left(\Delta t\right) = \begin{bmatrix} 4-3c & 0 & 0 & \frac{s}{n} & \frac{2(1-c)}{n} & 0 \\ 6(s-n\Delta t) & 1 & 0 & -\frac{2(1-c)}{n} & \frac{4s-3n\Delta t}{n} & 0 \\ 0 & 0 & c & 0 & 0 & \frac{s}{n} \\ 3ns & 0 & 0 & c & 2s & 0 \\ -6n(1-c) & 0 & 0 & -2s & 4c-3 & 0 \\ 0 & 0 & -ns & 0 & 0 & c \end{bmatrix} \tag{2.2}$$

where n signifies the mean motion of the passive vehicle, Δt is the time interval for propagation, and $s = \sin(n\Delta t)$ and $c = \cos(n\Delta t)$. In the filter, the mean motion in the equation above is actually computed as the angular rotation rate $(\dot{\theta})$ at the current time. In other words, the mean motion is chosen at each epoch to be the current along-track velocity of the passive vehicle divided by its radius. This provides a more accurate propagation for elliptical orbits as long as the measurement interval is not large.

The relative clock frequency is assumed constant over the time interval, so the clock terms are propagated with [16]

$$\Phi_{b,f}\left(\Delta t\right) = \begin{bmatrix} 1 & \Delta t \\ 0 & 1 \end{bmatrix}. \tag{2.3}$$

Thus, the full relative state transition matrix has the form

$$\Phi\left(\Delta t\right) = \begin{bmatrix} \Phi_{\mathbf{r},\mathbf{v}}\left(\Delta t\right) & \mathbf{0}_{6\times 2} \\ \mathbf{0}_{2\times 6} & \Phi_{b,f}\left(\Delta t\right) \end{bmatrix}. \tag{2.4}$$

Incorporated into the state propagation is velocity aiding, accomplished by using the $\Delta \mathbf{v}$ vectors of the active vehicle. The velocity vectors are added directly into the linear state propagation at the

given time as impulsive maneuvers, with potentially more than one maneuver between measurement epochs. The following example illustrates the equations for the occurrence of one $\Delta \mathbf{v}$ during the interval. As such, the state must be propagated from t_k to t_{k+1} with a maneuver at $t_{\Delta v}$ such that $t_k < t_{\Delta v} < t_{k+1}$. In this case, the state vector is propagated as follows:

$$\mathbf{s}_{\Delta v}^- = \mathbf{\Phi}\left(t_{\Delta v}, t_k\right) \mathbf{s}_k^+ \tag{2.5}$$

$$\mathbf{s}_{\Delta v}^+ = \mathbf{s}_{\Delta v}^- + \left[\mathbf{0}_{3\times 1}^T \; \Delta \mathbf{v}^T \; \mathbf{0}_{2\times 1}^T\right]^T \tag{2.6}$$

$$\mathbf{s}_{k+1}^- = \mathbf{\Phi}\left(t_{k+1}, t_{\Delta v}\right) \mathbf{s}_{\Delta v}^+ \tag{2.7}$$

where the $^-$ and $^+$ indicate state vector values before or after the measurement update or a maneuver. The distinction is clear from the context.

Not portrayed in the above equations is the fact that the CW state propagation is performed in cylindrical coordinates, with the along-track direction being along the arc of the orbit. Since this filter operates in the rectangular RIC coordinates, a rotation is performed to cylindrical RIC coordinates immediately before each state propagation step (e.g., Eq. 2.5), then back to rectangular immediately after. The equations for such a conversion are given in [17]. However, for this filter, those equations are re-derived for the case that $\dot{r}$ is not zero, providing a slight increase in accuracy.

Ignoring any potential maneuvers, the covariance is propagated over the entire measurement interval using

$$\mathbf{P}_{k+1}^- = \mathbf{\Phi}\left(t_{k+1}, t_k\right) \mathbf{P}_k^+ \mathbf{\Phi}\left(t_{k+1}, t_k\right)^T + \mathbf{Q}_k. \tag{2.8}$$

The process noise matrix $\mathbf{Q}$ is derived from Gelb, equation 3.6-13 [18],

$$\mathbf{\Gamma}_k \mathbf{Q}_k \mathbf{\Gamma}_k^T = \int\limits_{t_k}^{t_{k+1}} \mathbf{\Phi}\left(t_{k+1}, \tau\right) \mathbf{G}\left(\tau\right) \mathbf{Q}\left(\tau\right) \mathbf{G}^T\left(\tau\right) \mathbf{\Phi}^T\left(t_{k+1}, \tau\right) d\tau \tag{2.9}$$

where $\mathbf{Q}(t)$ is defined to be the spectral density matrix, and the corresponding discrete state equation is

$$\mathbf{s}_{k+1} = \mathbf{\Phi}_k \mathbf{s}_k + \mathbf{\Gamma}_k \mathbf{w}_k. \tag{2.10}$$

However, since the CW equations are used for state propagation, $\mathbf{w}_k$ is assumed to be zero mean, and $\boldsymbol{\Gamma}_k$ is assumed to be identity. If equal weighting is assumed, $\mathbf{G}(t)$ becomes an identity matrix, and Eq. 2.9 reduces to

$$\mathbf{Q}_k = \int\limits_{t_k}^{t_{k+1}} \boldsymbol{\Phi}\left(t_{k+1}, \tau\right) \mathbf{Q}\left(\tau\right) \boldsymbol{\Phi}^T\left(t_{k+1}, \tau\right) d\tau. \tag{2.11}$$

Eq. 2.11 is solved symbolically using Eq. 2.4 and a diagonal representation of the spectral density matrix $\mathbf{Q}(t)$.

2.3 Measurement Update

The RSKF performs a measurement update for each GPS observation separately, so the equations in this section refer to quantities for one common view GPS satellite. Given pseudorange observations to the same GPS satellite from the active receiver ρ_A and passive receiver ρ_P, the single difference observation is simply

$$\rho_{SD} = \rho_A - \rho_P. \tag{2.12}$$

The predicted single difference pseudorange $\tilde{\rho}_{SD}$ is computed from the geometric relative range, relative clock bias estimate, and antenna CG offsets. Because the pseudoranges in the above equation are measured from the GPS antennas, ρ_{SD} is not necessarily referenced to the centers of gravity of the two vehicles. Therefore, the prediction of the single difference pseudorange must account for the antenna CG offset vector $\mathbf{r}_{ANT}$. In the equations below, $\mathbf{r}_{ANT}$ can be viewed as the sum of the antenna offset vectors from the two vehicles. This assumes similar attitudes for the vehicles to promote common GPS constellation visibility.

The geometric relative range is found by differencing the ranges to the active and passive vehicles using the GPS satellite position $\mathbf{R}_{GPS}$, passive vehicle absolute position estimate $\mathbf{r}_P$, and predicted relative position estimate $\tilde{\mathbf{r}}_{REL}$ from the time update. The computed ranges to the active and

passive vehicle receivers are

$$\tilde{r}_P = |\mathbf{R}_{GPS} - \mathbf{r}_P| \tag{2.13}$$

$$\tilde{r}_A = |\mathbf{R}_{GPS} - (\mathbf{r}_P + \tilde{\mathbf{r}}_{REL} + \mathbf{r}_{ANT})|. \tag{2.14}$$

The predicted single difference is then computed from

$$\tilde{\rho}_{SD} = \tilde{r}_A - \tilde{r}_P + b_{REL}. \tag{2.15}$$

The single difference pseudorange residual is formed using

$$z = \rho_{SD} - \tilde{\rho}_{SD}. \tag{2.16}$$

The partial differential of Eq. 2.15 with respect to the relative state (Eq. 2.1) produces the measurement gradient matrix $\mathbf{H}$ with the first three elements being

$$H_{11} = -\frac{X_{GPS} - (x_P + \tilde{x}_{REL} + x_{ANT})}{\tilde{r}_A} \tag{2.17}$$

$$H_{12} = -\frac{Y_{GPS} - (y_P + \tilde{y}_{REL} + y_{ANT})}{\tilde{r}_A} \tag{2.18}$$

$$H_{13} = -\frac{Z_{GPS} - (z_P + \tilde{z}_{REL} + z_{ANT})}{\tilde{r}_A} \tag{2.19}$$

so that the full matrix is

$$\mathbf{H} = \begin{bmatrix} H_{11} & H_{12} & H_{13} & 0 & 0 & 0 & 1 & 0 \end{bmatrix}. \tag{2.20}$$

The Kalman gain is computed from the equation

$$\mathbf{K} = \mathbf{P}_{k+1}^{-}\mathbf{H}^T \left(\mathbf{H}\mathbf{P}_{k+1}^{-}\mathbf{H}^T + \mathbf{R}\right)^{-1} \tag{2.21}$$

and the covariance is updated with

$$\mathbf{P}_{k+1}^{+} = (\mathbf{I} - \mathbf{K}\mathbf{H})\,\mathbf{P}_{k+1}^{-}\,(\mathbf{I} - \mathbf{K}\mathbf{H})^T + \mathbf{K}\mathbf{R}\mathbf{K}^T. \tag{2.22}$$

Since the measurement update is performed for each GPS satellite separately, the measurement noise matrix $\mathbf{R}$ is 1×1, so the inversion in Eq. 2.21 is a simple scalar inversion.

Finally, the relative state is updated by

$$\mathbf{s}_{k+1}^{+} = \mathbf{s}_{k+1}^{-} + \mathbf{K}z. \tag{2.23}$$

The measurement update is repeated for each common view GPS satellite. After exhausting all the observations for this epoch, the next measurements are chosen and the entire process is repeated.

Chapter 3

Flight Test Results

3.1 STS-80 Flight Experiment

The STS-80 mission launched November 19, 1996, and returned to Earth December 7, 1996. During the mission, the Space Shuttle Columbia released the free-flying Orbiting and Retrievable Far and Extreme Ultraviolet Spectrograph Shuttle Pallet Satellite (ORFEUS SPAS). Both the SPAS and the Shuttle had GPS receivers on board, which were used to record concurrent observations for demonstration of relative navigation using GPS. The SPAS had a nine-channel Laben Tensor GPS receiver with four antennas, while the Shuttle used a six-channel Trimble Advanced Navigation System Quadrex GPS receiver with two antennas mounted across the payload bay [4].

The data set used to test the RSKF comprises the final 73 minutes of rendezvous, up to the capture (grapple) of the SPAS with the Shuttle robotic arm. Several data sets were taken throughout the mission, but only the rendezvous portion had a valid relative orbit truth reference. This segment of the experiment employed a laser on the Shuttle for determining range and range-rate to the SPAS. These data were converted into a best estimated relative trajectory (BERT) in radial, in-track, and cross-track (RIC) coordinates.

Because of the frequent thrusting of the Shuttle during rendezvous, the RSKF delta-V compensation is employed. The delta-V measurements were produced by the Shuttle IMU accelerometer, which reported accumulated sensed velocity [4]. Given Shuttle delta-V vectors expressed in RIC coordinates, implementation of velocity aiding in the filter is straightforward.

The rendezvous phase of the flight was performed in such as way as to maximize the potential for common view satellites. The Shuttle payload bay remained pointed at the SPAS so the crew could maintain visual contact; consequently, the SPAS was commanded to pitch at a constant rate so that its GPS antennas pointed in approximately the same direction as those on the Shuttle throughout the rendezvous [4].

3.2   Measurements

Both GPS receivers reported C/A code phase, L1 carrier phase, and L1 Doppler. The RSKF uses the C/A code pseudoranges from each common-view GPS satellite to create the single difference observation. The receivers were not synchronized, so the measurement time tags are different. Therefore, the pseudoranges from the active vehicle (Shuttle) receiver are interpolated to the times of the passive vehicle (SPAS) pseudoranges using polint.c, a polynomial interpolation routine from *Numerical Recipes* [19]. Polint.c uses Neville's algorithm to construct the interpolating polynomial. As implemented in the filter, the desired point is computed between the second and third values of a four-point interpolation.

It should be noted that both receivers maintain a clock bias between -0.5 and +0.5 ms, so the relative clock behavior for these receivers has steps of approximately 1 ms. The RSKF searches for these jumps by comparing the current single difference pseudorange to the previous one, which are approximately 300 km different if a receiver clock correction occurred. Also, neither the receivers nor the RSKF corrects the measurement time tags for the range bias, introducing an error that is

Table 3.1: Relative orbit position and velocity error statistics with respect to laser BERT for the Relative State Kalman Filter and the NASA/JSC filter [4].

		Position (m)			Velocity (cm/s)		
		Mean	STD	RMS	Mean	STD	RMS
RSKF	Radial	-2.8	5.8	6.4	-1.0	2.0	2.2
	In-Track	-4.2	3.2	5.3	-0.4	1.8	1.8
	Cross-Track	0.2	1.3	1.3	0.1	1.3	1.3
	RSS			8.4			3.1
JSC	Radial	-1.5	7.5	7.6	-2.0	8.7	8.9
	In-Track	-2.6	2.9	3.9	0.0	6.1	6.1
	Cross-Track	-0.2	2.9	2.9	-1.2	4.0	4.2
	RSS			9.0			11.6

most likely below the noise level.

3.3 Results

Given noisy, asynchronous observations from the drag-laden, maneuvering Shuttle and the relatively well-behaved SPAS, the RSKF obtains excellent results considering its simplicity. In fact, the results are comparable or better than results obtained in a NASA/JSC study detailed in [4]. Table 3.1 shows the position and velocity error statistics for the same 73 minute period using the same truth reference (the laser BERT) for the RSKF and for the filter developed by JSC. The JSC filter estimates the relative state by differencing absolute orbit estimates of each vehicle. When at least four common-view satellites are visible, the JSC filter solves for the orbits with only those in common view, using the same filter-estimated range bias for a given GPS SV. If less than four common satellites are in view, all channels are processed for both receivers [4].

The RSKF results are obtained with the following initial variances: 4000, 1000, and 100 m^2 for RIC relative position; 0.004, 0.004, and 0.001 m^2/s^2 for RIC relative velocity; 2000 m^2 for relative clock bias; and 25 m^2/s^2 for relative clock frequency. The initial spectral densities are as follows:

1e-5, 4e-6, 8e-6 m^2/s for RIC relative position; 3e-7, 4e-8, 8e-8 m^2/s^3 for RIC relative velocity; 0.01 m^2/s for relative clock bias; and 0.008 m^2/s^3 for relative clock frequency. The noise on the measurement is estimated to be approximately 3 m, so the scalar measurement noise value $\mathbf{R}$ is set to 9 m^2. It becomes apparent in subsequent plots that additional tuning must be performed so that the filter 3σ RMS values more accurately reflect the behavior of the system.

To illustrate the nature of the rendezvous, Figs. 3.1, 3.2, and 3.3 show the relative position and velocity states. The in-plane relative trajectories for the filter and laser BERT are shown in Fig. 3.1. Note that motion is to the right and the Earth is down. It can be seen from this plot that the rendezvous data set begins at a range of approximately 1.8 km and ends at SPAS capture. Figs. 3.2 and 3.3 show all the relative position and velocity states as determined by the RSKF and the laser BERT. These plots reveal the large dynamic motion of the Shuttle during the first fifteen minutes as it narrows the relative range from 1.8 km to 200 m. After the first fifteen minutes, the relative motion becomes more benign, but is still difficult to model because the Shuttle is maintaining its position along the R-bar. That is, the Shuttle is matching the velocity of the SPAS from a lower altitude.

Another indicator of the large motions at the beginning of the data set is the plot of the delta-V magnitudes in Fig. 3.4. For the purpose of velocity aiding in the RSKF, a range of minimum thresholds was evaluated. A threshold of 1.5 cm/s was determined to provide the best accuracy. The figure shows a line at 1.5 cm/s, with the points above it marked by squares to indicate those used in state propagation.

The relative position errors with respect to the laser BERT in the radial, in-track, and cross-track directions are shown in Fig. 3.5. The 3σ bounds determined by the RSKF variances are shown as the dashed lines. Fig. 3.6 shows the relative velocity errors with respect to the laser BERT. Again, the 3σ bounds determined by the filter variances are shown as the dashed lines. Compare the behavior of these error plots with the motion shown in Figs. 3.2 and 3.3. Clearly,

the RSKF has difficulty obtaining accurate results during the highly dynamic motion of the first fifteen minutes, even with velocity aiding. After that period, however, the filter estimates become less erratic.

Notice the biases and systematic variations in the relative position error for the radial and in-track directions. These are reflected in the mean and RMS position error statistics in Table 3.1. Possible sources of error include inaccurate GPS antenna CG offsets, time tagging errors, or simply unknown/unmodeled biases. The fact remains, however, that these biases can be removed by adjusting the body-fixed antenna CG offsets by the bias amount. Doing so lowers the position RMS errors to the same level as the standard deviations, thereby reducing the total RSS position error from 8.4 m to 6.9 m. There is only a minimal improvement in the velocity statistics.

To ensure that the RSKF CW propagation is not introducing a bias to the results, a hardware-in-the-loop simulation of a 50 km baseline used in [1] was used to verify its accuracy. Details given in the next chapter show unbiased results. The results do show a an error due to relative J2 for the 50 km baseline, but that should not be an issue with this much smaller baseline. Clearly, the source of the bias in the Shuttle/SPAS data set requires further investigation.

The most dramatic result from this data set is the improvement in relative velocity estimates by the RSKF versus the JSC results. The RSKF total RSS velocity error of 3.1 cm/s is a 73% improvement over the 11.6 cm/s value from JSC (see Table 3.1). Both filters include velocity aiding using the Shuttle IMU accelerometer data. In fact, both filters use virtually the same data, so the improvement in velocity accuracy is most likely an artifact of using single difference observations in the RSKF.

Finally, the plots of clock behavior are given in Figs. 3.7 and 3.8. Fig. 3.7 shows the estimates of clock bias and frequency from the RSKF and from GEODE, the absolute orbit determination utility used in conjunction with the RSKF. The difference of these estimates is shown in Fig. 3.8. The statistics on the error plot reflect values after the first five minutes. Also, the statistics for the

bias error include extreme outliers that occur near the steps of 1 ms shown in Fig. 3.7. If outliers greater than 100 μs are omitted (21 of 1981 points), the RMS error drops to less than 1 μs.

These two plots reflect the need for a more accurate clock model in the RSKF. Long outages in GPS data are obvious from the sections of constant frequency in Fig. 3.7. Corresponding bias errors can be seen Fig. 3.8. While frequency may be considered constant over spans of seconds, the assumption quickly becomes invalid for outages of minutes. More appropriate clock models are currently being evaluated.

3.4   Conclusion

In a relatively simple form, the RSKF has demonstrated on flight data the ability to predict relative position and velocity to accuracy levels comparable to or better than the absolute state filter developed by NASA/JSC. Further improvements in positioning accuracy may be obtained by identifying the source of the relative position estimate biases, which appear in both the RSKF and the JSC filter results to differing degrees. There is also the potential for additional overall improvements in accuracy by implementing a relative state propagator that accounts for the effects of relative gravity and drag perturbations. The most dramatic improvement, however, is gained by using more precise observations and techniques, namely carrier phase processing coupled with synchronization of the vehicle clocks. The potential of the RSKF with synchronous and much more accurate measurements is shown in the next chapter.
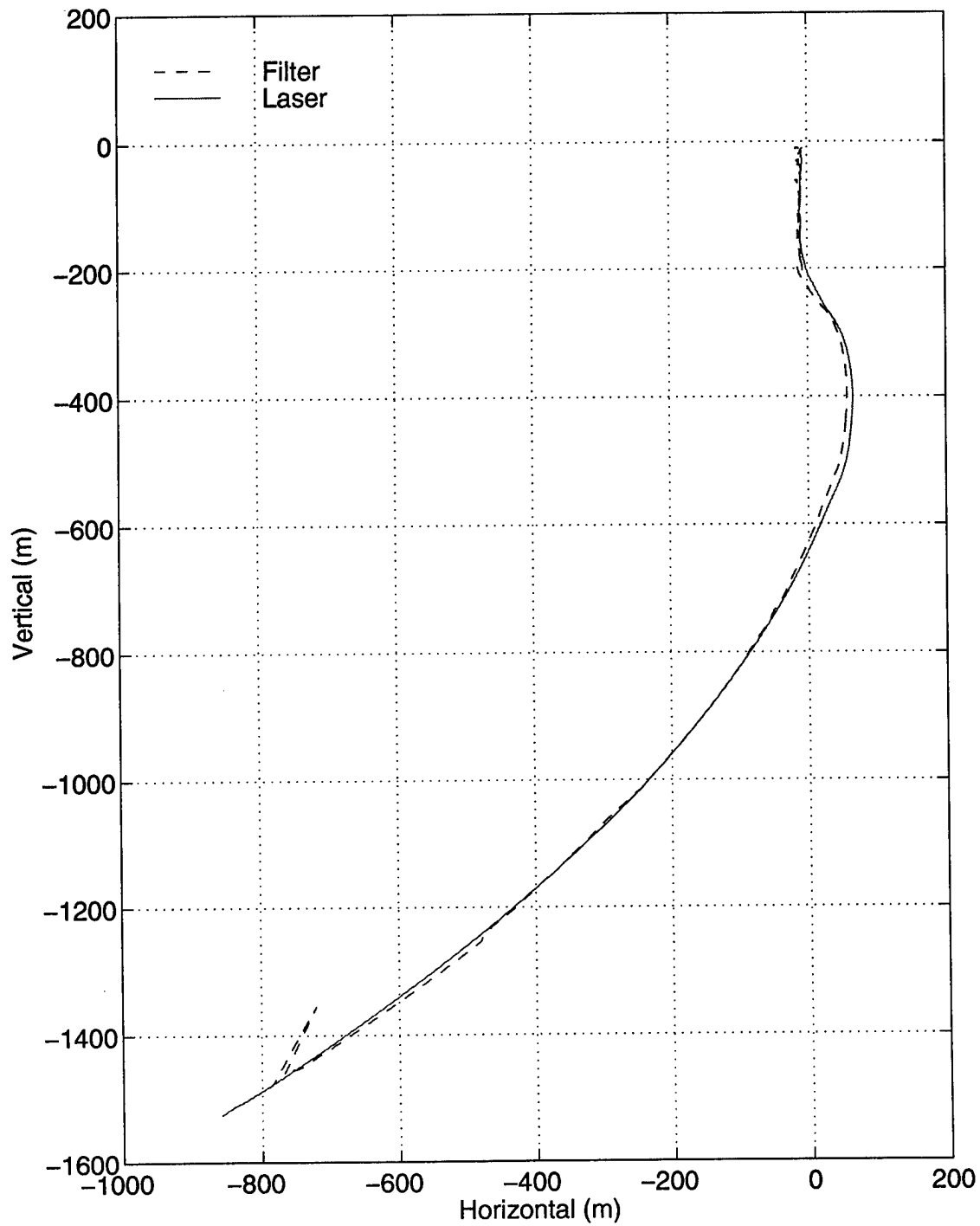
Figure 3.1: In-plane trajectories for filter and laser BERT.
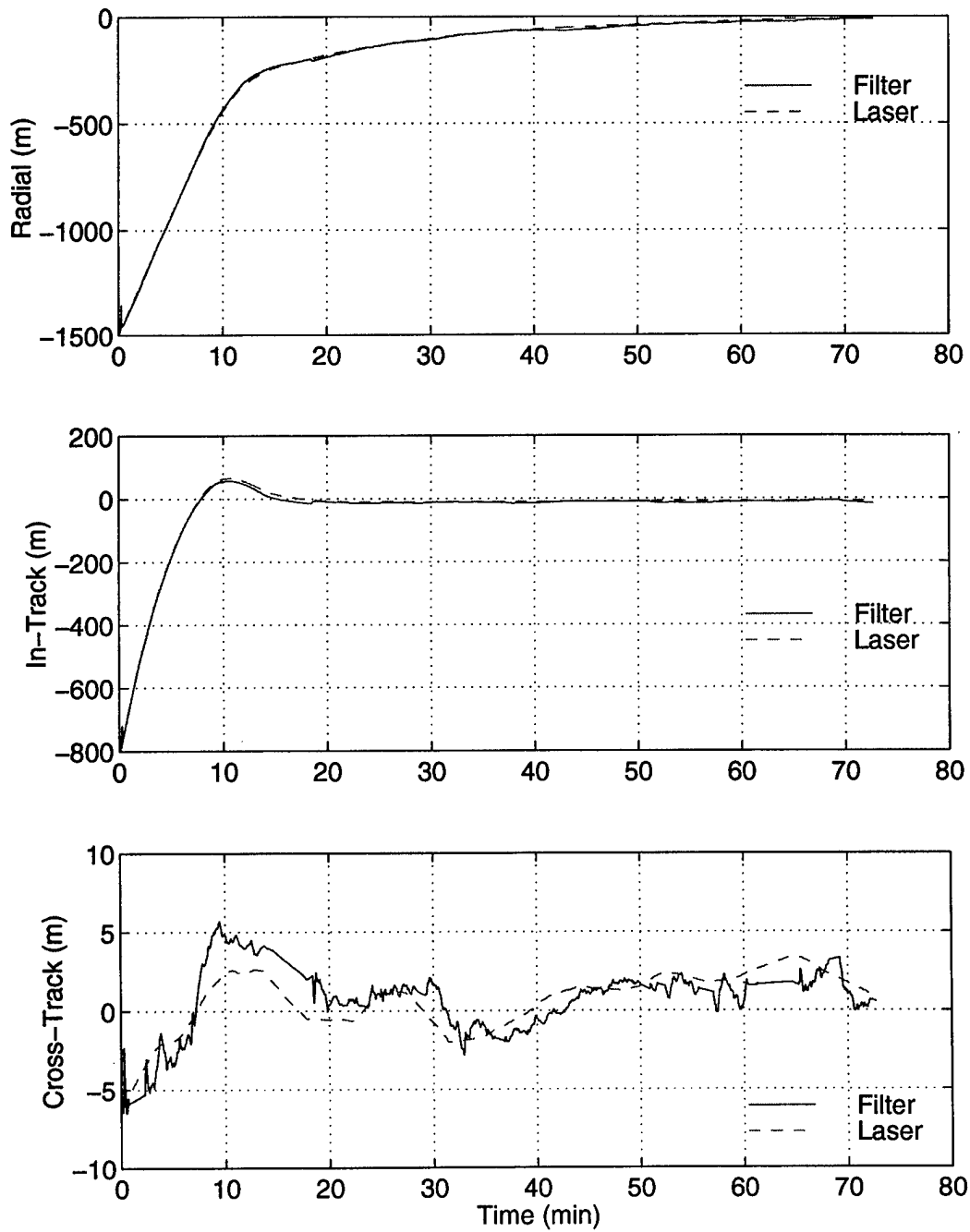
Figure 3.2: Radial, in-track, and cross-track relative positions for the filter solutions and laser BERT.
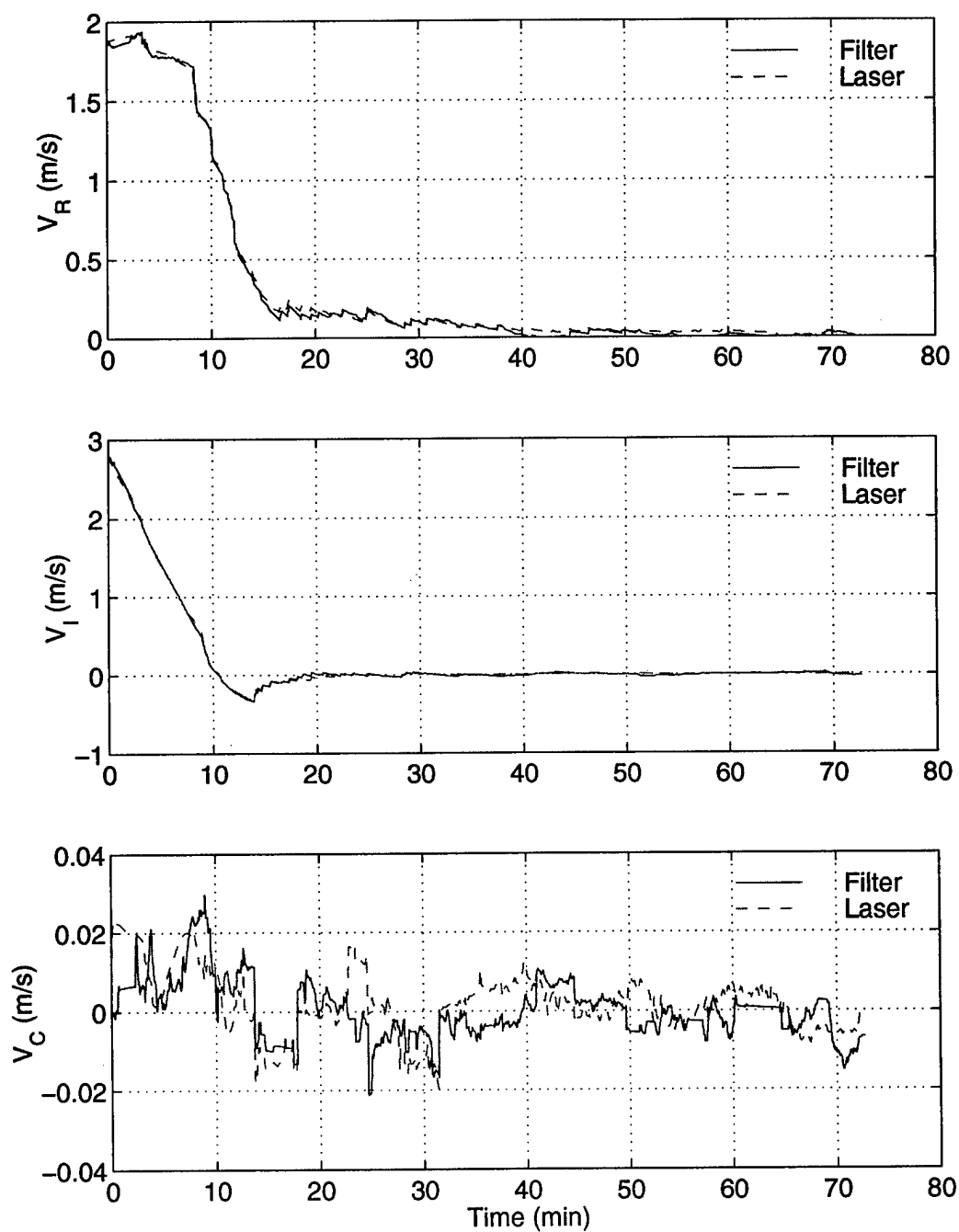
Figure 3.3: Radial, in-track, and cross-track relative velocities for the filter solution and laser BERT.
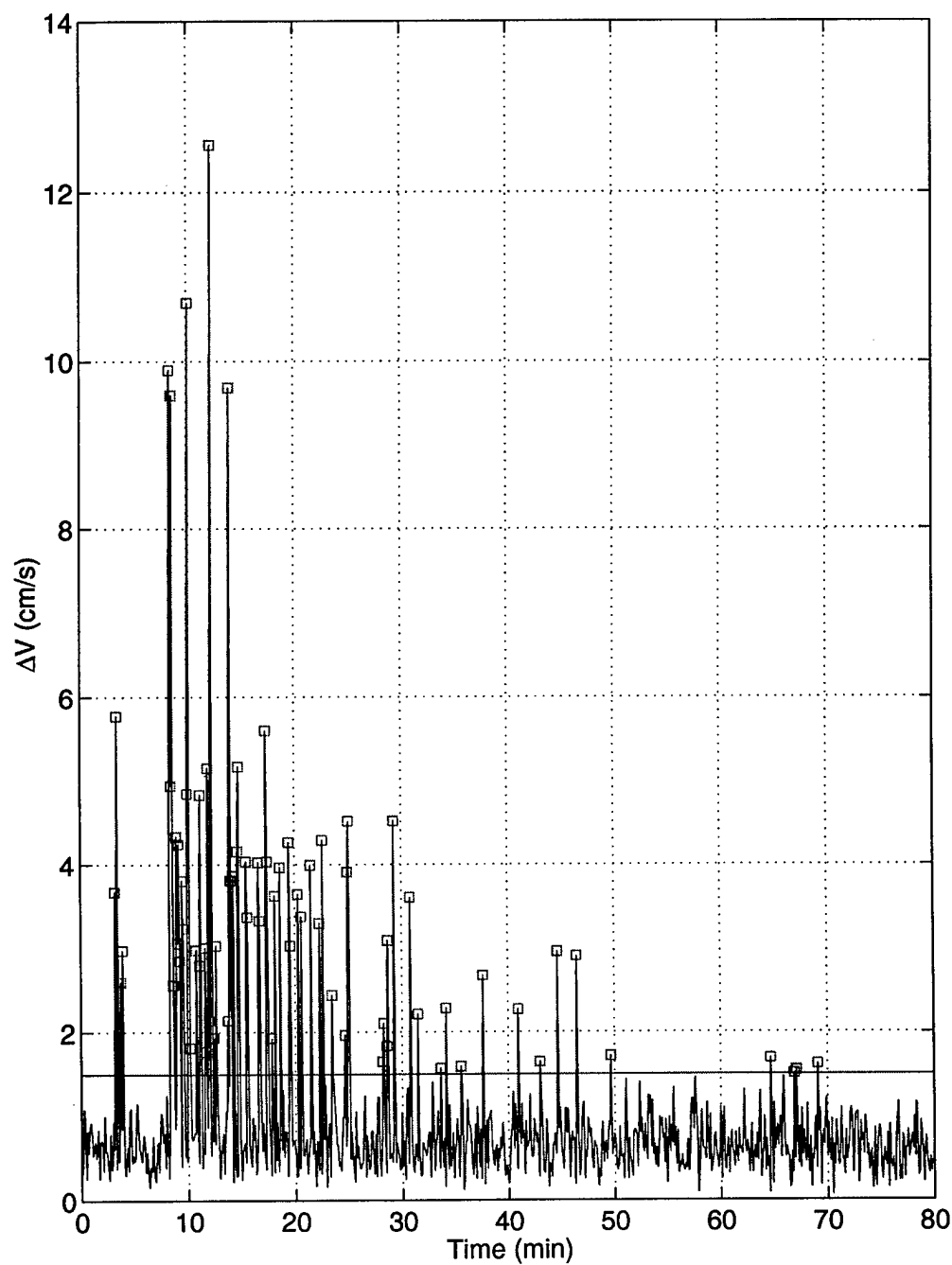
Figure 3.4: Shuttle IMU-sensed ΔV magnitudes. Threshold of 1.5 cm/s is shown, with squares signifying the points used in state propagation.
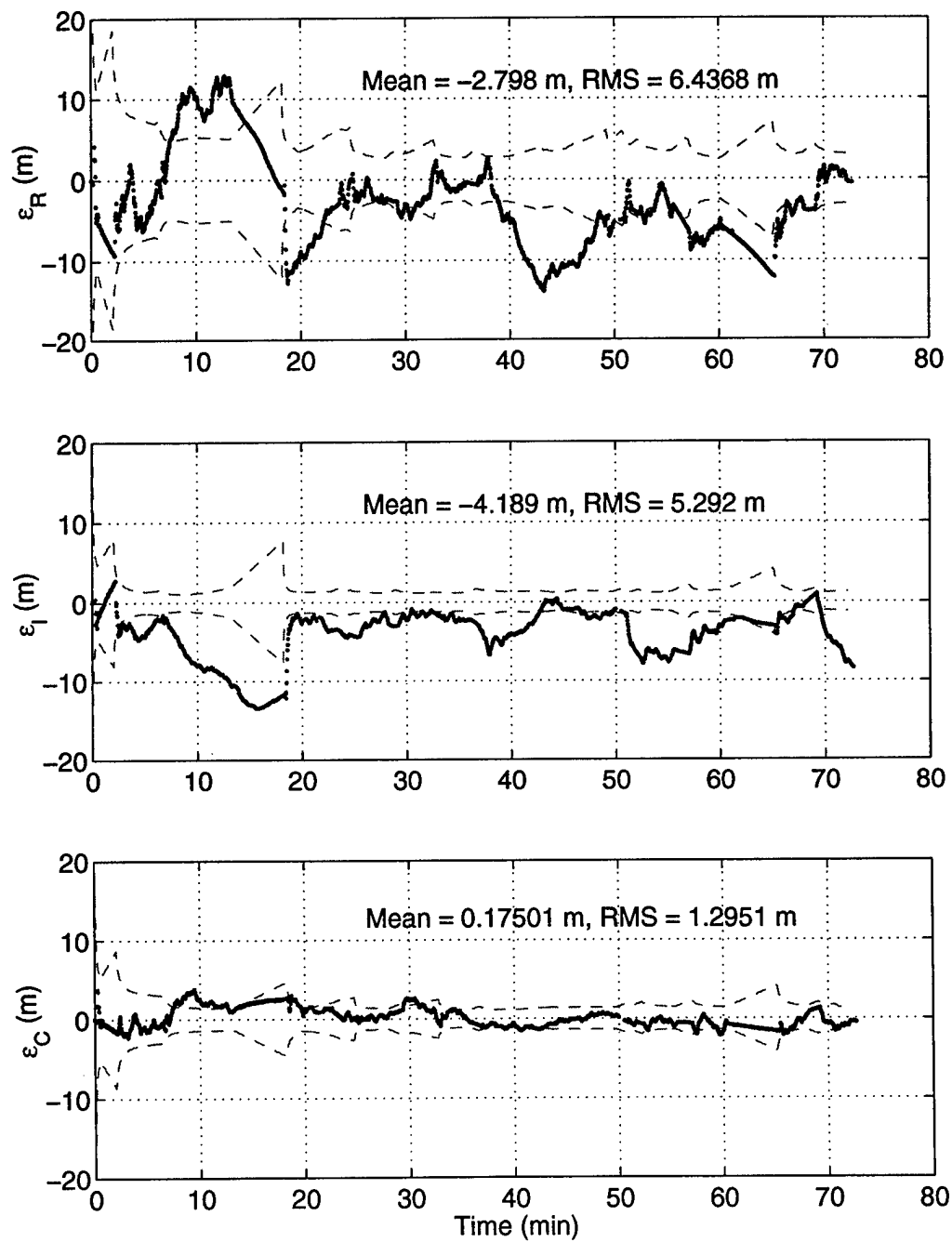
Figure 3.5: Relative position error in radial, in-track, and cross-track directions with respect to laser. Dotted lines show filter 3σ formal error.
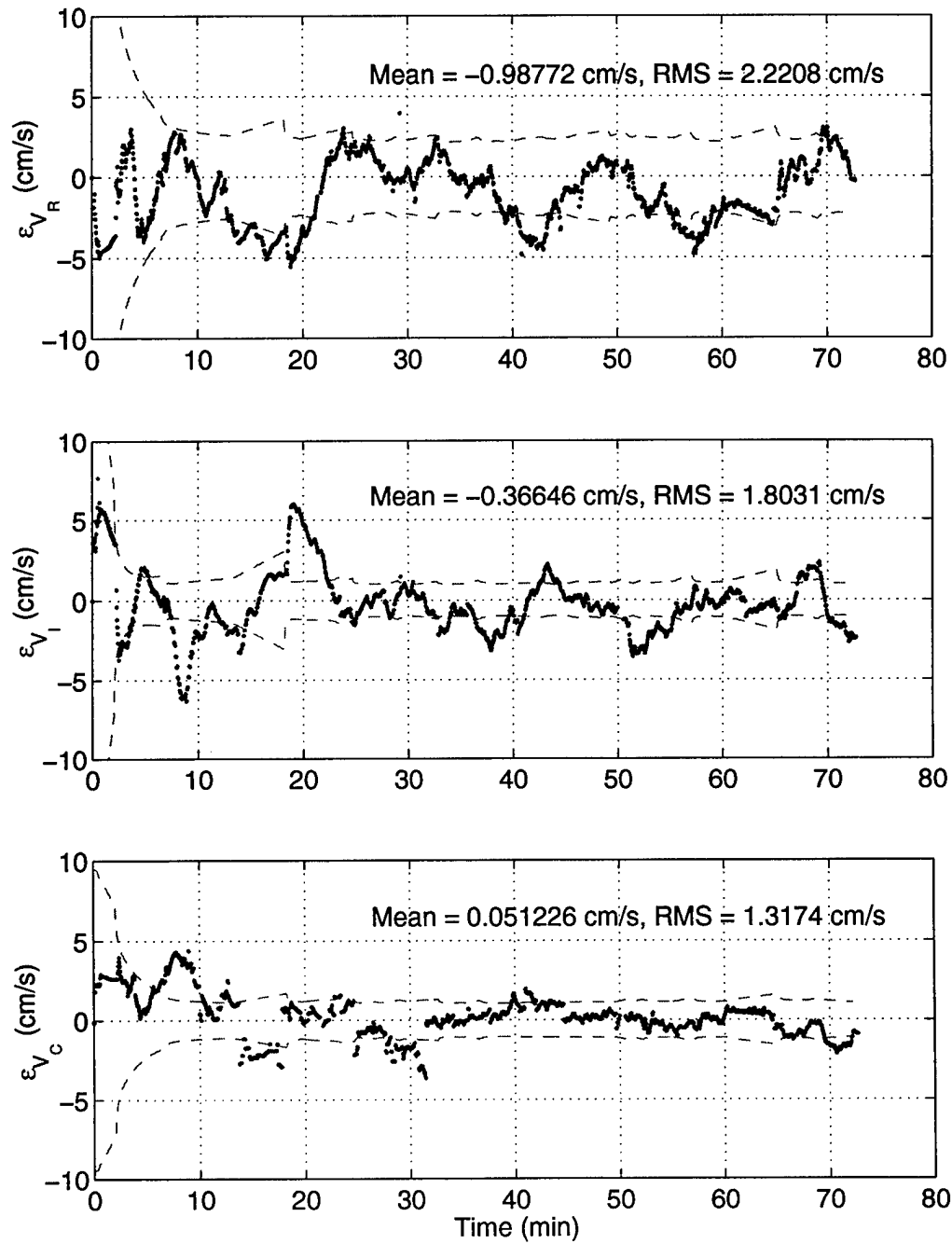
Figure 3.6: Relative velocity error in radial, in-track, and cross-track directions with respect to laser. Dotted lines show filter 3σ formal error.
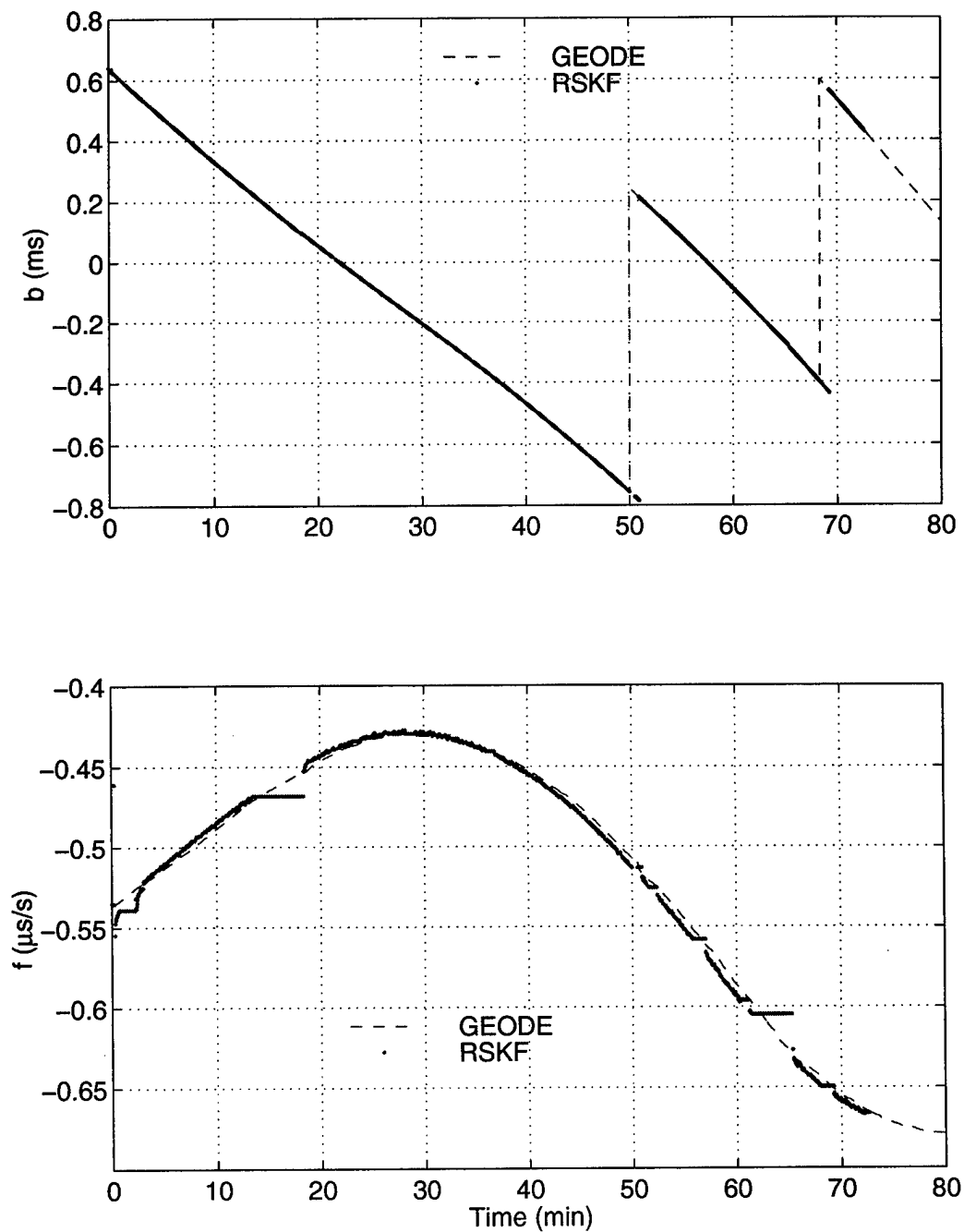
Figure 3.7: Relative clock bias and frequency estimates from GEODE absolute OD utility and from RSKF. Both receivers adjust their clocks to stay within 0.5 ms of GPS time. Note the outages in GPS data where frequency from RSKF becomes constant.
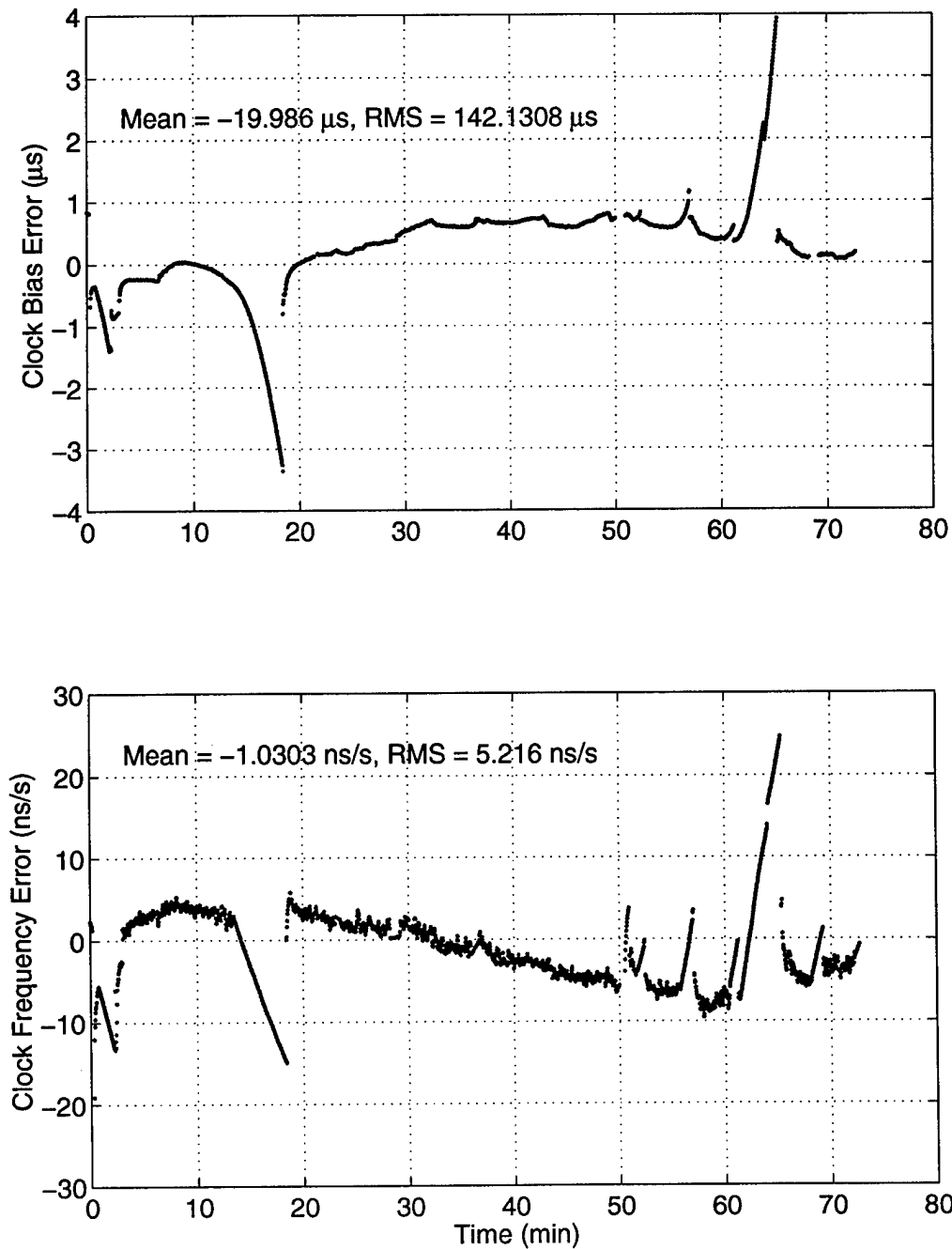
Figure 3.8: Relative clock bias and frequency comparison between GEODE and RSKF estimates. Statistics do not include first 5 minutes. Bias statistics include extreme outliers that occur near the steps (see Fig. 3.7).

Chapter 4

Hardware Simulation Results

Because the Shuttle/SPAS data include large maneuvers and noisy data, it is difficult to gauge the potential accuracy of the RSKF from those results. Therefore, I ran a simplified version of the RSKF on hardware simulated data prepared by Patrick Binning at NRL. The simulation includes no maneuvering, so the maneuver compensation portion of the RSKF algorithm is not utilized. Moreover, Binning provided data sets pre-processed through the NRL orbit determination utility OCEAN with time tags already aligned, so measurement interpolation is not necessary in the RSKF. Finally, no antenna CG offsets are modeled, so that feature of the RSKF is also not utilized here. What remains to test is the core of the RSKF: the CW propagation model and the measurement equations.

The details of the hardware simulations can be found in [1]. The results shown in this chapter are from only one of the many simulations. Binning models a Front and Back satellite for each simulation. The Back satellite follows the Front with along-track separations of generally 5, 50, or 500 km. The scenario given here is for a separation of 50 km, with initial orbit elements given in Table 4.1. The GPS data are collected from an Allen Osborne Associates TurboRogue receiver attached to a Northern Telecom GPS RF signal simulator (an earlier version of the simulator to

Table 4.1: Initial orbital elements for 50-km separation hardware simulation performed by Binning [1].

a	7063.145 km
e	0.001
i	66.05 deg
Ω	0.0 deg
ω	0.0 deg
M (Front)	270.162 deg
M (Back 50 km)	269.756 deg
Epoch Date: Sept. 20, 1996	
YUMA Constellation: GPS Wk 871	

be used in the time transfer hardware simulation). Binning set every controllable error source including ionosphere to zero, so there is very little noise on the measurements.

The observations input to the RSKF are L1 P-code pseudoranges output from OCEAN with corrected time tags. The pseudoranges for both receivers are also interpolated to the nearest integer second within OCEAN, allowing explicit differencing in the RSKF. Input to the RSKF also includes the OCEAN ephemeris for the target vehicle and GPS SV positions at the measurement times. Of the 9.5-hour data set, I processed a section of approximately 2.5 hours that has good common visibility of the GPS constellation.

4.1 Results

Table 4.2 shows summary statistics of the results as compared to the truth output from the simulation. The statistics do not include the first 20 minutes during which the filter converges. The corresponding relative position and velocity error plots are shown in Figs. 4.1 and 4.2. Table 4.2 shows that the RSS relative position error is only 26.1 cm for the 50 km separation distance. On the other hand, there is a relatively large cross-track velocity error that causes the RSS relative velocity error to be almost 5 cm/s. While the in-plane RMS velocities are both around 0.4 cm/s,

Table 4.2: Relative orbit position and velocity error statistics with respect to simulation truth for the Relative State Kalman Filter for 50 km separation.

	Position (cm)			Velocity (cm/s)		
	Mean	STD	RMS	Mean	STD	RMS
Radial	-4.5	18.0	18.6	0.03	0.41	0.41
In-Track	-4.1	12.3	12.9	0.02	0.37	0.37
Cross-Track	3.9	12.4	13.0	-1.36	4.56	4.75
RSS			26.1			4.78

the RSKF appears to have difficulty resolving the relative cross-track motion.

For comparison of the errors to their relative state values, Figs. 4.3 and 4.4 show the relative position and velocity, respectively, for both the RSKF (solid) and truth (dotted). Not surprisingly, the most notable feature is the difference in cross-track relative velocity estimates. According to the RSKF, there is essentially no cross-track relative motion, while the truth state is oscillating with the period of the orbit to a maximum of 6 cm/s. The most likely cause of this discrepancy is a relative J2 effect. For a 50 km along-track separation distance, the relative J2 effect will be the difference of small accelerations at low geocentric latitudes, and the difference of larger accelerations at high geocentric latitudes. Correspondingly, the times when the true relative cross-track velocity is zero correspond to a geocentric latitude of zero; whereas, the times of maximum relative cross-track velocity correspond to maximum geocentric latitude.

This result highlights a limitation of the current RSKF implementation with a simple linear CW model and no velocity dependence in the measurement equation (Eq. 2.15). This effect does not show up in the Shuttle/SPAS solution because of the close proximity of the vehicles (within 500 m for most of the time). Compensation for the relative J2 effect, however, should improve the results on data sets with relatively large separations.

Another feature to note in Fig. 4.1 is the correlation between the increase in formal position error and the decrease in common GPS satellites in view, shown in Fig. 4.5. The number of

common-view SVs drops to three near the 22 min, 45 min, and 60 min marks, with successively

longer durations. Note the corresponding increases in formal position error, particularly in the

radial direction. Other portions of the 9.5-hour data set include worse common visibility (including

no common satellites), at which point the solution begins to diverge. This sensitivity of the RSKF

(or OCEAN absolute) position estimates to less than four common-view satellites requires further

investigation.

Fig. 4.6 shows a comparison of the RSKF relative clock estimates to the difference of the

OCEAN absolute estimates. No truth reference for clock bias and frequency exists for this hardware

simulation, so the comparison is made to results from another filter. The relative clock estimates

themselves are shown in Fig. 4.7. Note the huge relative frequency step in Fig. 4.7. Due to the

existence of that step, the process noise for that state must be large, as indicated by the large formal

error in the frequency error plot of Fig. 4.6. Also, the factor of 40 step causes range residuals so

large that the RSKF residual editor never recovers. Therefore, the residual editing feature is not

implemented for this data set. This unexpected frequency behavior highlights another area for

improvement in the RSKF. The residual editing scheme must be enhanced to allow residual editing

while suffering only short outages due to anomalous behavior.

4.2   Conclusion

The low noise and large separation of this simulated data allows better evaluation of the filter

algorithms than the Shuttle/SPAS flight data. While the results indicate a couple shortcomings of

the algorithms, what is also clear is that the RSKF in its current state can resolve relative positions

to less than 20 cm in each direction over a 50 km baseline. Furthermore, with compensation for

relative J2, these results indicate that relative velocity could be resolved to 0.4 cm/s or better

in each direction. Carrier phase processing should improve the results even further, though not

dramatically because of the low noise on the P-code pseudoranges. In summary, the RSKF provides

accurate results for most states, but requires modification to improve the accuracy of the cross-track relative velocity.
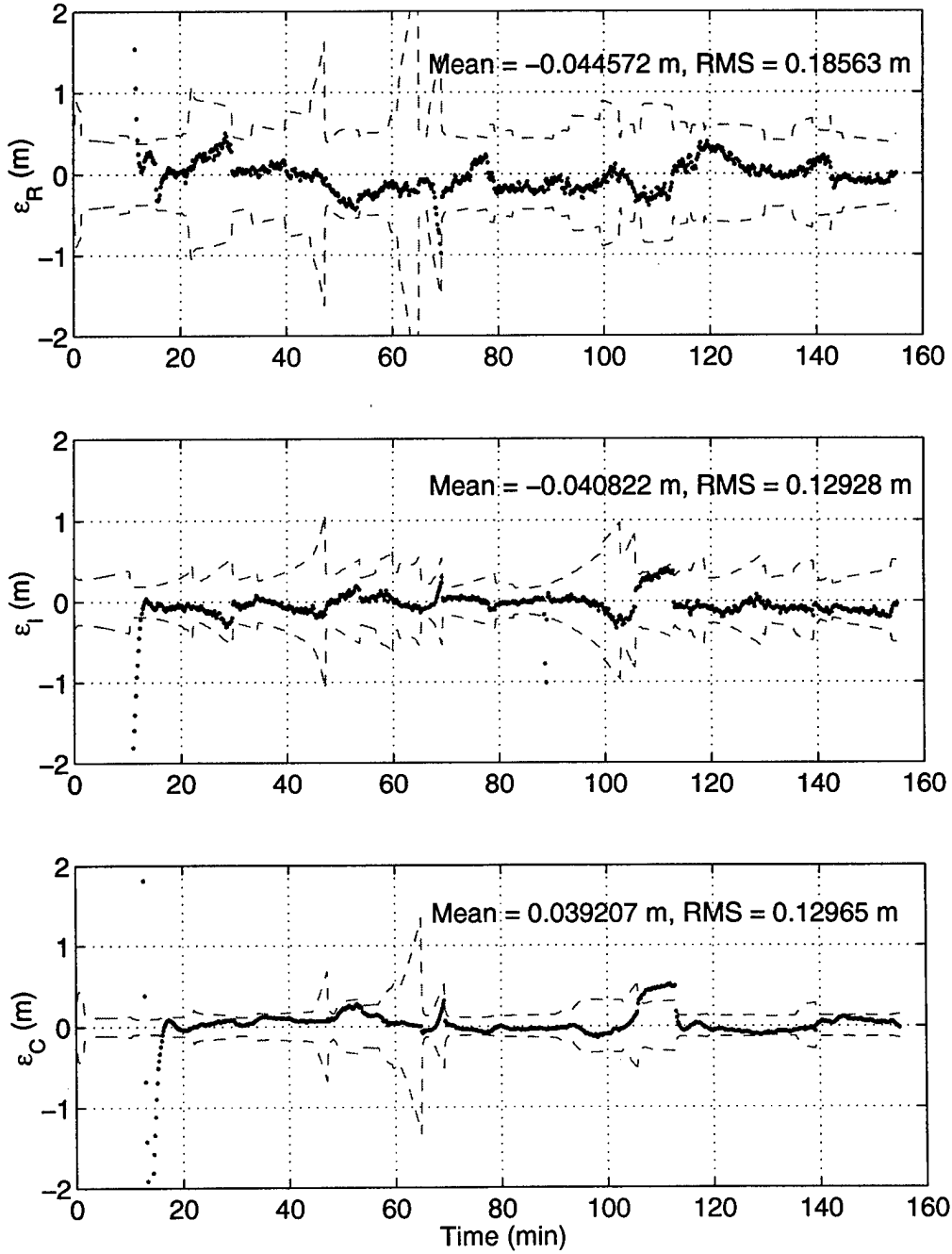
Figure 4.1: Radial, in-track, and cross-track relative position errors for the RSKF with respect to simulation truth. Dotted lines show filter 1σ formal error.

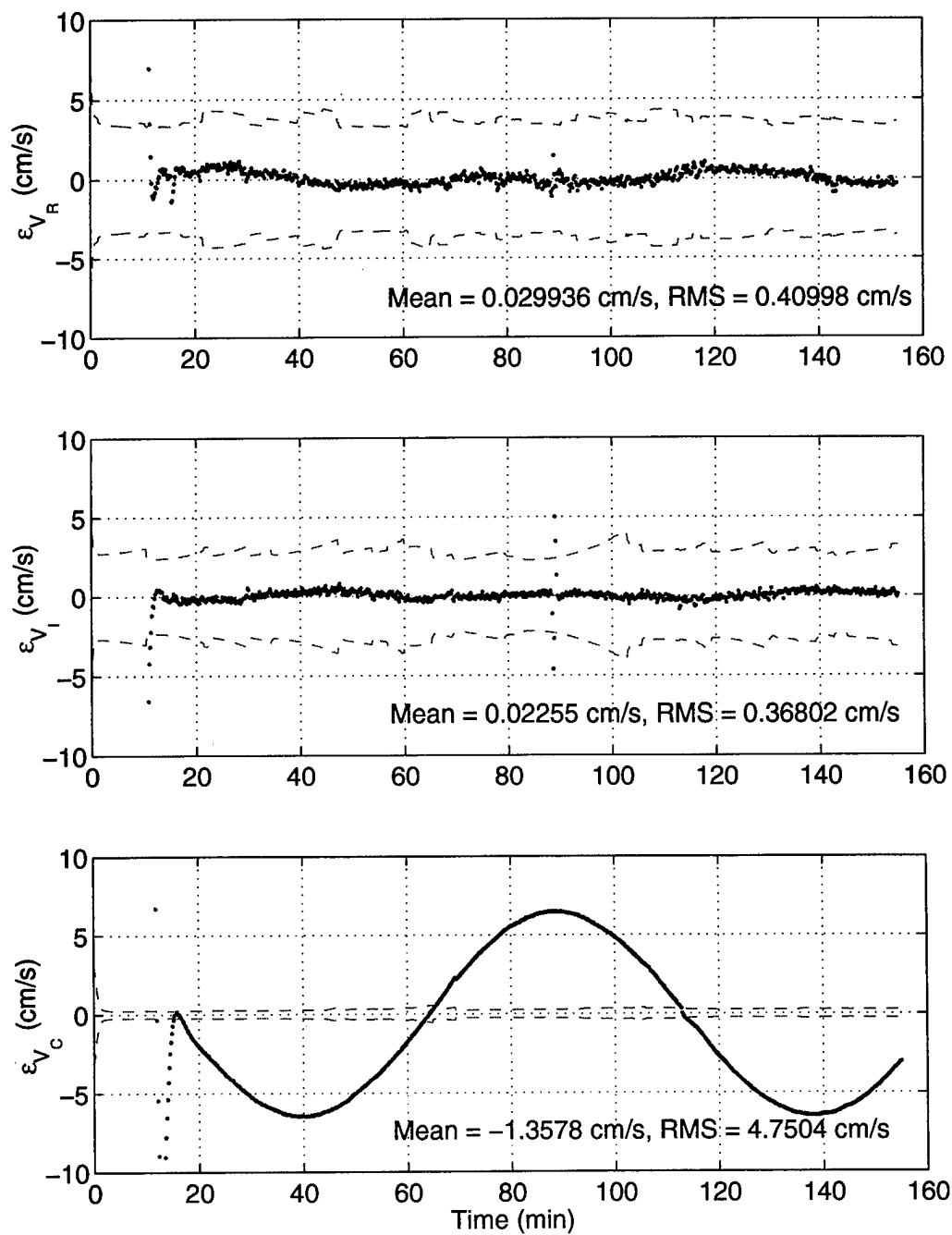Figure 4.2: Radial, in-track, and cross-track relative velocity errors for the RSKF with respect to simulation truth. Dotted lines show filter 1σ formal error.
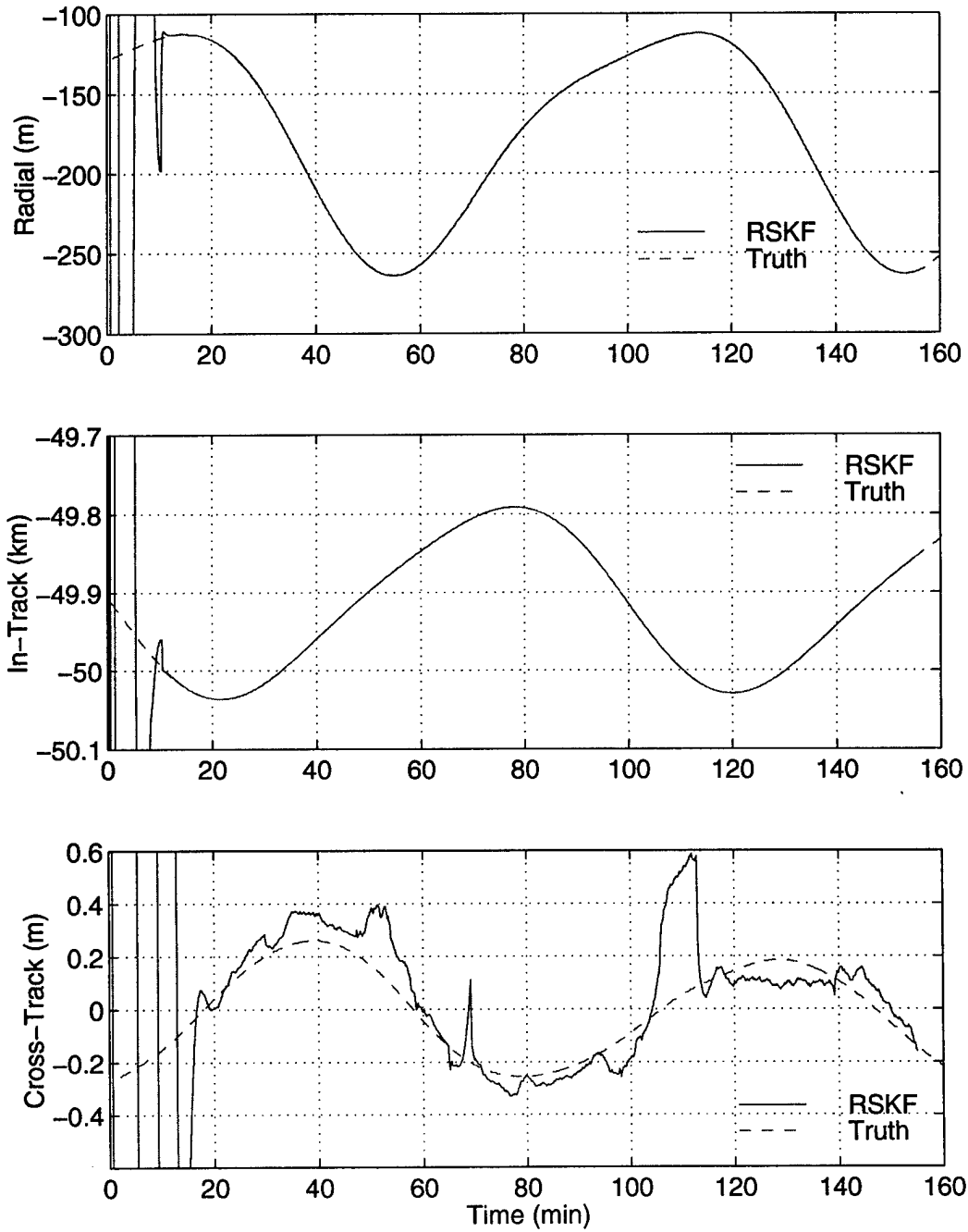
Figure 4.3: Relative position in radial, in-track, and cross-track directions for RSKF and truth. Note that the scale on the in-track ordinate is km.
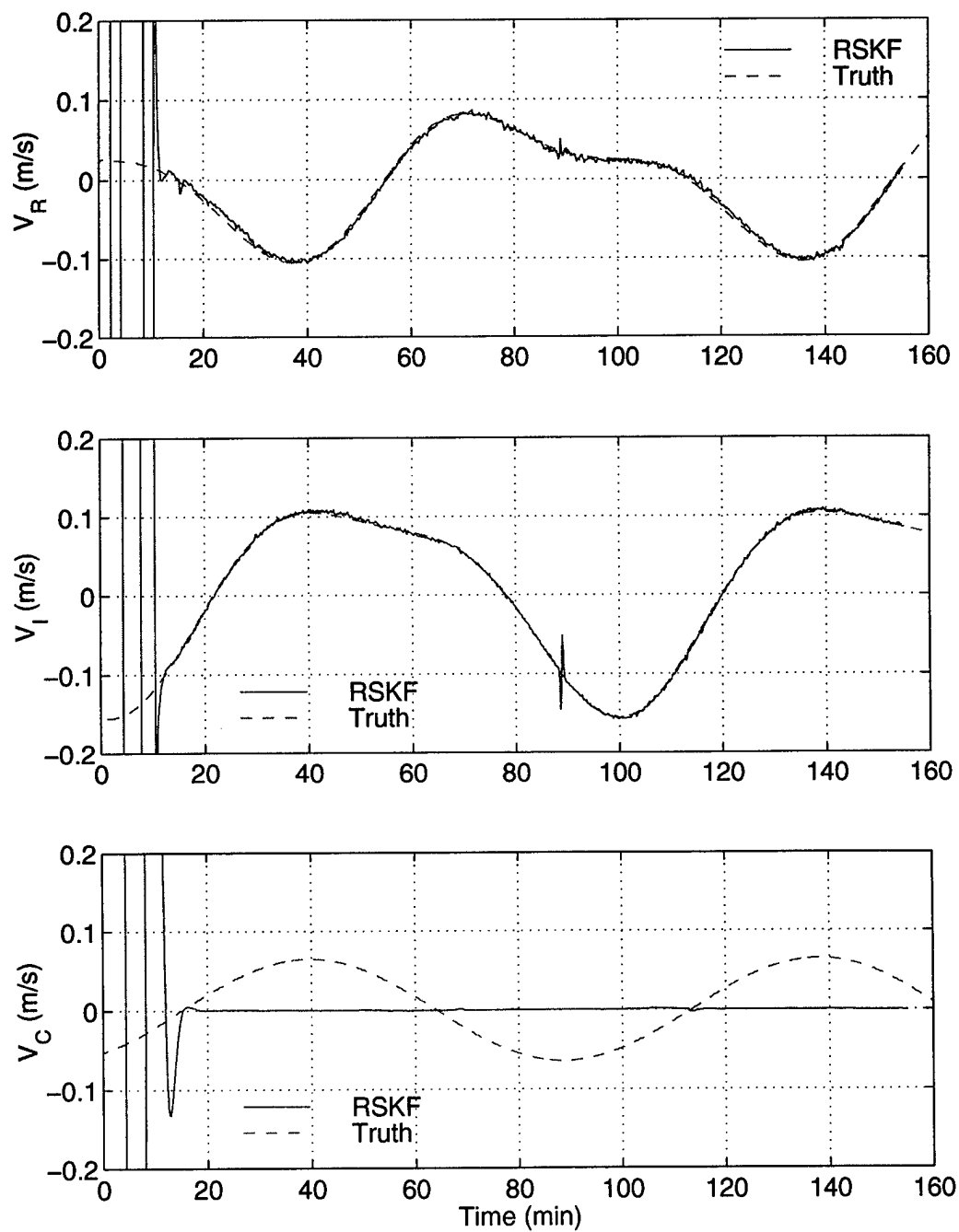
Figure 4.4: Relative velocity in radial, in-track, and cross-track directions for RSKF and truth.
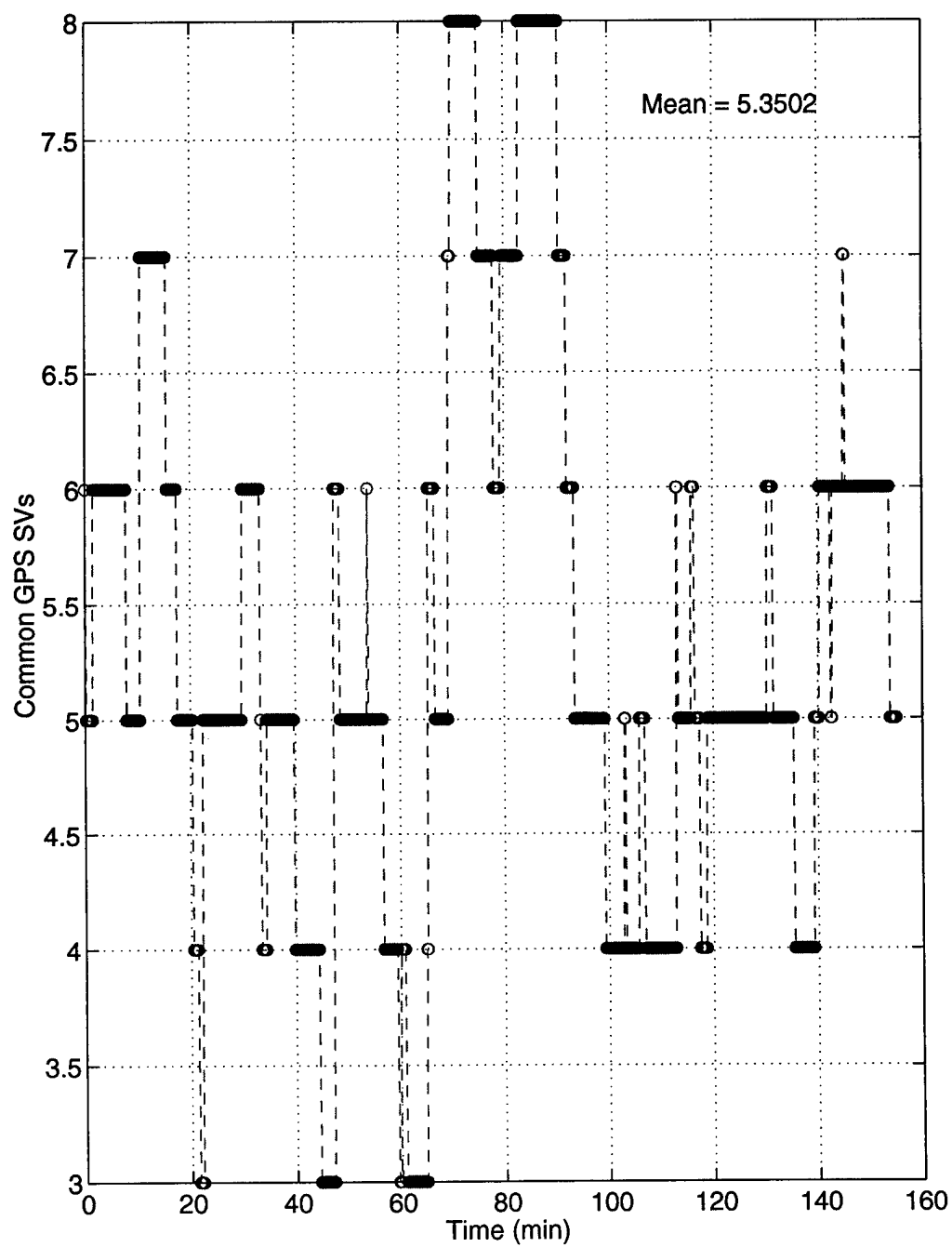
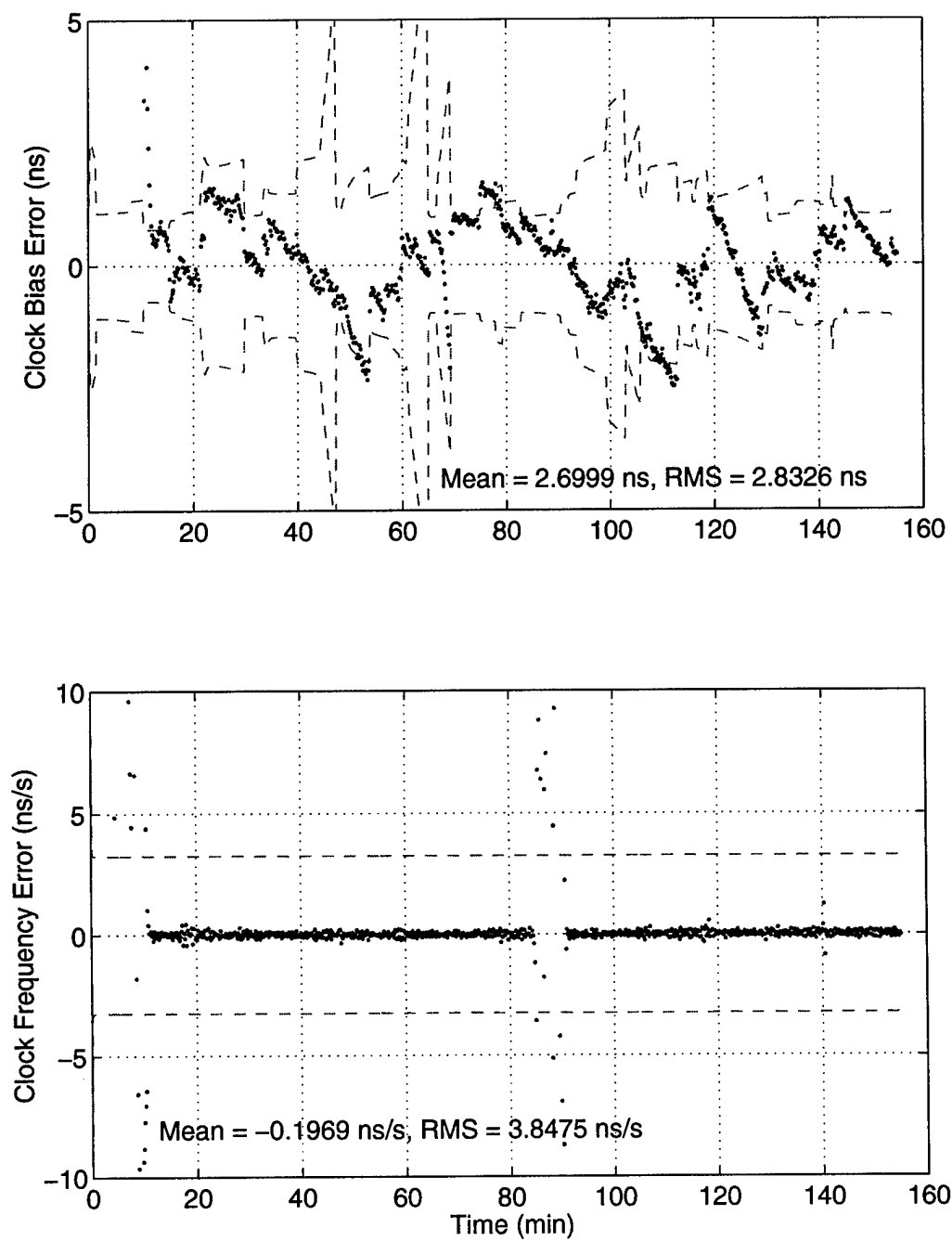Figure 4.5: Common GPS SV visibility for 50 km separation.

Figure 4.6: Relative clock bias and frequency errors for RSKF with respect to difference of absolute clock states from NRL OCEAN estimates. Dotted lines show filter 1σ formal error. Mean clock bias error is subtracted out.
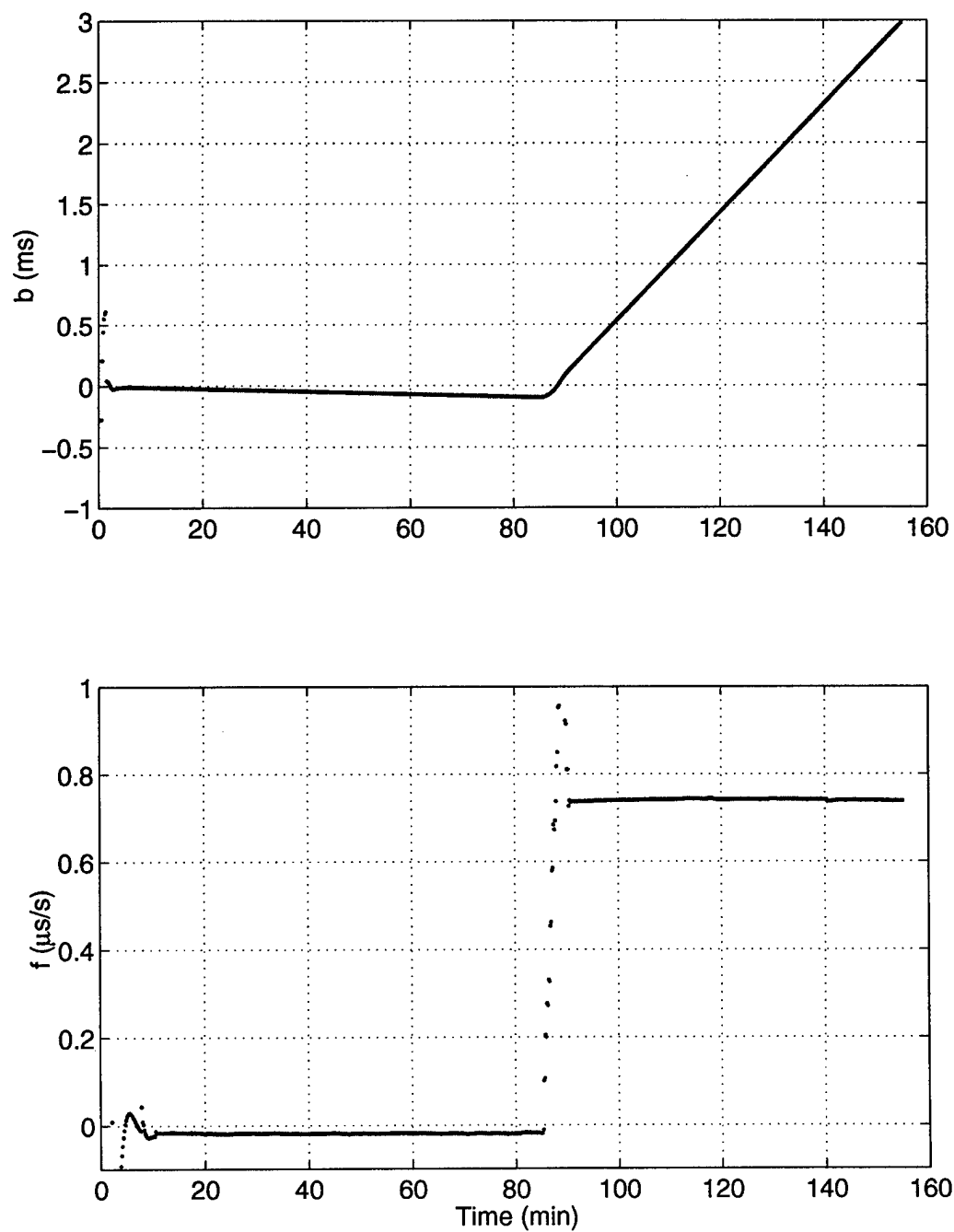
Figure 4.7: Relative clock bias and frequency states from RSKF.

Chapter 5

Time Transfer Hardware Simulation

The algorithms for on-orbit relative navigation, timing, and frequency will be tested primarily using newly-generated hardware-in-the-loop simulations which will include a truth reference for the clock states. The following sections describe the hardware to be used in the test bed and the procedures for testing.

5.1 Test Bed

Fig. 5.1 represents the basic test bed for two GPS receivers being tested in parallel. Two Global Simulation Systems (GSS) GPS signal simulators will provide simultaneous signals to separate Trimble Advanced Navigation Sensor (TANS) six-channel GPS receivers. The two receivers will be modeled in neighboring orbits. The 1 pulse-per-second (PPS) output from each receiver will be measured in both an absolute and a relative sense by interval counters. A hydrogen maser operating at 5 MHz will provide an accurate reference oscillator signal to the simulators as well as to the interval counters. The maser will also provide a reference 1 PPS signal to the interval counter measuring the absolute accuracy of the receiver clocks. Knowledge of the absolute clocks
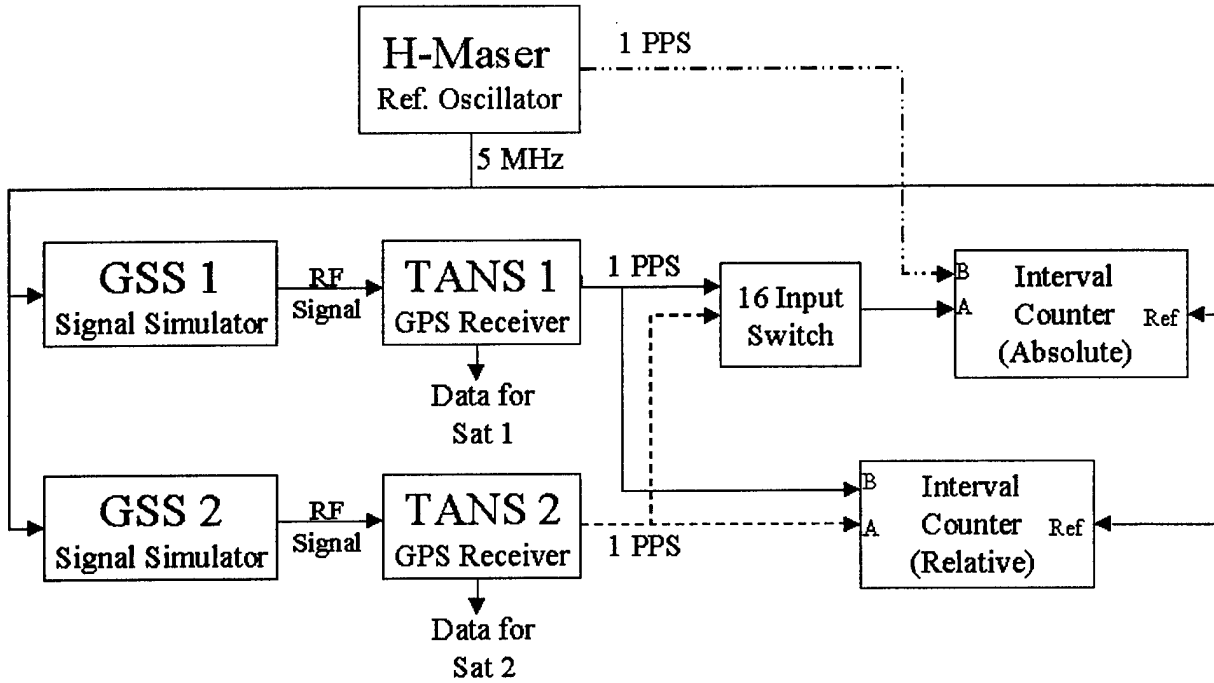
43

Figure 5.1: Time transfer test bed. Absolute and relative measurement of the 1 PPS out of the GPS receivers is actually performed in separate runs of identical simulations.

is desired to help identify any anomalous relative behavior.

The GSS simulators produce a comprehensive development and testing environment. The simulator consists of Multichannel Satellite Signal Source (MSSS) and a host computer. The MSSS is the actual hardware unit that generates the RF signals sent to the receiver. The signal generator can be considered a pseudorange-to-RF converter [20]. The host computer drives the MSSS and processes the results of the simulation. The GSS software allows specification or adjustment of almost (if not) all parameters of the simulation. Some examples are spacecraft characteristics, dynamics limits, antenna details, orbit initial conditions or ephemeris, maneuvers, attitudes, ionosphere, multipath, and GPS constellation configurations and signal strengths. NRL is currently running version 6.46 of the GSS firmware, versus version 1.20 when Binning performed his simulations [1].

The Trimble receiver is a six-channel, Standard Positioning Service (SPS) receiver which uses the C/A code on L1. The stated PPS output has a width of 1 microsecond with the falling edge

synchronized to UTC within 1 microsecond [21]. In a conversation with Joe White of NRL, he indicated that the resolution of the TANS PPS should be better, approximately 100 nanoseconds absolute. Although not as precise as desired, the benefit of using the TANS is the fact that NRL has two. This allows synchronous simulation as portrayed in Fig. 5.1. If only one receiver is used, separate tests must be performed, making synchronization and measurement of relative clock behavior problematic. Also, if two different receiver types are used, that requires processing two different receiver output formats.

Future tests, however, may include the Motorola GPSR dual-frequency, twelve-channel receiver developed for NRL. These tests may be performed in series or in parallel with a TANS, at which point the limitations mentioned above must be overcome. The outcome of preliminary tests with the TANS receivers will help determine the direction of future testing.

5.2 Test Plan

The test bed depicted in Fig. 5.1 actually comprises two simulation runs. Due to potential impedance problems caused by splitting the PPS output from the GPS receivers, the exact same simulation scenario will be run twice, once to measure the absolute clock behavior and again to measure the relative clock behavior. The relative clock behavior cannot be determined accurately from the absolute measurements because they are not taken simultaneously. The interval counter samples the channels of the switch unit only every 5 minutes. However, with the PPS output from the receivers plugged directly into the interval counter during the second run, measurements of relative clock behavior can be taken at 1 Hz.

Simulations with varying baselines will be run. Because the TANS receiver can see only a maximum of six satellites, separation distances greater than several hundred kilometers may not include a sufficient number of common-view GPS satellites. The first tests will include separation

distances of 10 km and 100 km with both along-track and cross-track initial offsets. All specifiable error sources will be set to zero for the initial tests so that the C/A code pseudoranges from the TANS are as noiseless as possible. The measured relative clock bias and frequency will be evaluated for sufficient precision before proceeding. Assuming small-enough time resolution, the data will be processed with the RSKF, and the filter models and algorithms will be adjusted to achieve the highest possible precision.

If the TANS proves unreliable, the most likely course of action is to employ the Motorola GPSR receiver in series simulations. The task of obtaining an accurate truth reference for the relative clock behavior will be worked out with the help of committee members and the timing experts at NRL. If neither GPS space receiver can resolve time to the desired precision, then my research will attempt to estimate the relative clock states to the measured precision.

5.3   Conclusions

Successful completion of this research will produce the first demonstration of precise relative navigation and timing of satellites in orbit in real time using actual hardware data. This capability will permit applications such as synchronization of observations from a distributed system of sparse aperture radar satellites. Another contribution will be the design of the test bed for simultaneous hardware simulation of co-orbiting vehicles and measurement of the absolute and relative clock behavior. This will be a useful tool for analyzing the relative navigation and timing performance of GPS receivers for future formation flying architectures. Overall, this will be an interesting research topic with the potential to produce valuable new tools for satellite-to-satellite navigation and time transfer.

Bibliography

[1] Binning, P. W., *Absolute and Relative Satellite to Satellite Navigation Using GPS*. Ph. D. Dissertation, University of Colorado, 1997.

[2] Upadhyay, T., et al., "Precision Relative Navigation for Automated Rendezvous and Docking," 22nd Annual AAS Guidance and Control Conference, February 3-7, 1999.

[3] Cox, D. B., Jr., and Brading, J. D. W., "Integration of LAMBDA Ambiguity Resolution with Kalman Filter for Relative Navigation of Spacecraft," Institute of Navigation 55th Annual Meeting, June 28-30, 1999.

[4] Schiesser, E., Brazzel, J. P., Carpenter, J. R., Hinkel, H. D., "Results of STS-80 Relative GPS Navigation Flight Experiment," *Proceedings of AAS/AIAA Space Flight Mechanics Meeting*, Paper AAS 98-194, Vol. 99, Part II, 1998.

[5] D'Souza, C., et al., "An Evaluation of the GPS Relative Navigation System for ETS-VII and HTV," 22nd Annual AAS Guidance and Control Conference, February 3-7, 1999.

[6] Mokuno, M., Kawano, I., Kasai, T., "Experimental Results of Autonomous Rendezvous Docking on Japanese ETS-VII Satellite," 22nd Annual AAS Guidance and Control Conference, February 3-7, 1999.

[7] Cox, D. B., Jr., and Brading, J. D. W., "GPS Autonomous Relative Navigation and Time Transfer for Orbiting Space Vehicles," *Proceedings of ION GPS 95*, Sept. 12-15, 1995, pp. 217-228.

[8] Cox, D. B, Jr., and Brading, J. D. W., "GPS Navigation and Time Transfer for Pairs of Orbiting Space Vehicles," *Proceedings of the ION National Technical Meeting*, Jan. 14-16, 1997, pp. 417-428.

[9] Klepczynski, W. J., "GPS for Precise Time and Time Interval Measurement," *Global Positioning System: Theory and Applications, Volume II*, B. W. Parkinson and J. J. Spilker, Jr., Eds. American Institute of Aeronautics and Astronautics, Washington, D. C., 1996, Ch. 17, pp. 483-500.

[10] Lewandowski, W., Azoubib, J., and Klepczynski, W. J., "GPS: Primary Tool for Time Transfer," *Proceedings of the IEEE*, Vol. 87, No. 1, Jan. 1999, pp. 163-172.

[11] Allan, D. W., Ashby, N., and Hodge, C., "A Brief History of Precise Time and GPS," Supplement to *GPS World* Magazine. Advanstar Communications, Dec. 1998.

[12] Allan, D. W., and Weiss, M. A., "Accurate Time and Frequency Transfer During Common-View of a GPS Satellite," *Proceedings of the 34th Annual Frequency Control Symposium*, May 1980, pp. 334-346.

[13] Levine, J., "Time Transfer Using a Multi-Channel Code-Based GPS Receiver," *Proceedings 1998 IEEE International Frequency Control Symposium*, Pasadena, CA, pp. 284-291.

[14] Larson, K. M., and Levine, J., "Carrier-Phase Time Transfer," *IEEE Transactions on Ultrasonics, Ferroelectrics, and Frequency Control*, Vol. 46, No. 4, July 1999, pp. 1001-1012.

[15] Prussing, J. E., and Conway, B. A., *Orbital Mechanics*. Oxford University Press, New York, 1993.

[16] Parkinson, B. W., and Spilker, J. J., Jr., eds., *Global Positioning System: Theory and Applications Volume I*. American Institute of Aeronautics and Astronautics, Washington, DC, 1996.

[17] Bond, V. R., "A New Solution for the Rendezvous Problem," Paper AAS-99-178, AAS/AIAA Space Flight Mechanics Meeting, February 7-10, 1999.

[18] Gelb, A., ed., *Applied Optimal Estimation*. The M.I.T. Press, Cambridge, 1974.

[19] Press, W. H., et al., *Numerical Recipes in C: The Art of Scientific Computing*. Cambridge University Press, Cambridge, 1992.

[20] *STR Series Multichannel Satellite Navigation Simulator: Reference Manual*, Global Simulation Systems, Issue 8.00, May 1999.

[21] *TANS Trimble Advanced Navigation Sensor 6-Channel GPS Receiver: Specification and User's Manual*, Trimble Navigation Limited, Part Number 17035, Rev. B, March 1991.

REPORT DOCUMENTATION PAGE

Public reporting burden for this collection of information is estimated to average 1 hour per response, including the time for reviewing instructions, searching existing data sources, gathering and maintaining the data needed, and completing and reviewing the collection of information. Send comments regarding this burden estimate or any other aspect of this collection of information, including suggestions for reducing this burden, to Washington Headquarters Services, Directorate for Information Operations and Reports, 1215 Jefferson Davis Highway, Suite 1204, Arlington, VA 22202-4302, and to the Office of Management and Budget, Paperwork Reduction Project (0704-0188), Washington, DC 20503.

1. AGENCY USE ONLY *(Leave Blank)*	2. REPORT DATE February 17, 2000	3. REPORT TYPE AND DATES COVERED Final Report 1 Sep 1997 - 31 Aug 1999

4. TITLE AND SUBTITLE Spaceborne Differential GPS Applications	5. FUNDING NUMBERS GRANT NO: N00014-97-1-G025 PR NO. 81-0337-97

| 6. AUTHORS Penina Axelrad Dolan Highsmith Angela Reichert | |

7. PERFORMING ORGANIZATION NAME(S) AND ADDRESS(ES) University of Colorado, CB 431 Colorado Center for Astrodynamics Research Boulder, CO 80309	8. PERFORMING ORGANIZATION REPORT NUMBER PA-99-305

9. SPONSORING / MONITORING AGENCY NAME(S) AND ADDRESS(ES) Department of the Navy Naval Research Laboratory 4555 Overlook Ave S.W. Washington, D.C., 20375-5326	10. SPONSORING / MONITORING AGENCY REPORT NUMBER

11. SUPPLEMENTARY NOTES

12a. DISTRIBUTION / AVAILABILITY STATEMENT APPROVED FOR PUBLIC RELEASE	12b. DISTRIBUTION CODE

13. ABSTRACT *(Maximum 200 words)*

This final technical report summarizes the research performed by the Colorado Center for Astrodynamics Research (CCAR) for the Naval Research Laboratory (NRL) on Spaceborne Differential GPS Applications over the period 01 September 1997 through 31 August 1999. The primary focus of our work was on relative state estimation using GPS data from two vehicles. Data from a spaceborne experiment conducted by NASA was used for algorithm development and performance analysis. An auxiliary area of research was the identification and reduction of multipath errors in GPS observations. This effort is key to full utilization of GPS for high precision applications such as attitude determination, differential GPS, and relative navigation. The report comprises three documents describing the research. The first two are conference papers presented at ION GPS 99 describing the relative navigation and multipath research. The third is a doctoral dissertation research proposal written by Dolan Highsmith, summarizing his research on this project and plans for future work.

14. SUBJECT TERMS GPS, Relative Navigation, Multipath			15. NUMBER OF PAGES 68
			16. PRICE CODE

17. SECURITY CLASSIFICATION OF REPORT UNCLASSIFIED	18. SECURITY CLASSIFICATION OF THIS PAGE UNCLASSIFIED	19. SECURITY CLASSIFICATION OF ABSTRACT UNCLASSIFIED	20. LIMITATION OF ABSTRACT UL

NSN 7540-01-280-5500

Standard Form 298 (Rev. 2-89)
Prescribed by ANSI Std. Z39-1
298-102